Laser-Induced Line-Narrowing Effects in Coupled Doppler-Broadened Transitions. II. Standing-Wave Features*

B. J. Feldman and M. S. Feld
Physics Department, Massachusetts Institute of Technology, Cambridge, Massachusetts 02139
(Received 29 March 1971; revised manuscript received 21 October 1971)

Previous theoretical results on the influence of a laser on the line shape of a coupled transition—laser-induced line narrowing—have been restricted to the case where the laser is detuned from the center of its atomic gain profile or is in the form of a traveling wave. This paper extends those results to include the case where the laser is an intense standing-wave field tunable to the center of its atomic gain profile (conditions for Lamb dip). The effect may be observed either in transmission, by probing the coupled transition with a weak traveling-wave field coaxial with the laser field, or else in spontaneous emission from the coupled transition viewed along the axis of the laser field. It is now well known that for a laser detuned from the center of its atomic gain profile, two narrow Lorentzian resonances of different widths appear superimposed upon the broad background signal at frequencies symmetrically located about the corresponding line center. When the laser is tuned to the center of its gain profile, however, additional fine structure develops. This structure, which is particularly significant when the laser field is intense, may have important applications in high-resolution spectroscopy and laser-frequency stabilization. In this paper the laser frequency may be smaller or larger than the frequency of the coupled transition. In the latter case an intense laser introduces additional splitting effects, even when the laser is detuned. Splitting effects due to weakly saturating laser fields are also discussed. The problem is formulated by expanding elements of the ensemble-averaged density matrix in an infinite series of spatial Fourier components. A perturbation technique is employed, valid for a weak probe field and a standing-wave field of arbitrary intensity. One obtains an expression for emission induced by the probe field due to atoms moving with one velocity, written in terms of continued fractions in the general case and with Bessel functions in an important special case. This expression is integrated over the atomic velocity distribution by means of a computer to obtain the total emission due to atoms moving with all velocities. In some cases the integrated expressions may be written in closed algebraic form. A detailed discussions of line shapes and of the physical processes involved is included.

I. INTRODUCTION

The line shape of a Doppler-broadened transition is dramatically altered by the presence of a standing-wave laser field resonating with a second Doppler-broadened transition sharing a common level [Fig. 1(a)]. For a laser detuned from the center of its atomic gain profile, two narrow Lorentzian resonances of different widths appear superimposed upon the broad background signal of the coupled transition at frequencies symmetrically located about its line center [Fig. 1(b)].[1-6] Recent observations of this effect,[7-11] called "laser-induced line narrowing," confirm the predictions of the theory. The line-narrowing produced, which can be 100–1000 times narrower than the Doppler background, has been utilized in a variety of ways as a high-resolution spectroscopic technique for determining isotope shifts,[12] fine[13] and hyperfine[11,14,15] structure, g factors,[14,16] and linewidth parameters.[17-19] The effect may be observed either in transmission, by probing the coupled transition with a weak traveling-wave field coaxial with the laser field, or else in spontaneous emission from the coupled transition viewed along the axis of the laser field (Fig. 2). Note that identical line shapes will be observed in both cases since the spontaneous emission line shape is equivalent to the line shape of emission induced by a probe field containing a single photon in each mode.[4]

The over-all features of the line-narrowing effect may be understood in terms of the velocity selection of moving atoms by the standing-wave laser field. The field selectively interacts with atoms whose velocities Doppler-shift one of its traveling-wave components into resonance. This produces changes in the laser-level populations over two narrow intervals symmetrically located about the center of the velocity distribution. These changes reflect themselves in the gain profile of the coupled transition. The above explanation does not account for the different widths of the two change signals, nor, as shall be seen, for the other striking line-shape features to be described below. The formulation, analysis, and interpretation of these effects form the content of this paper.

Previous theoretical results[1-6] on the influence of the laser on the line shape of a coupled transition have been limited to the case where the laser is detuned from the center of its atomic gain profile

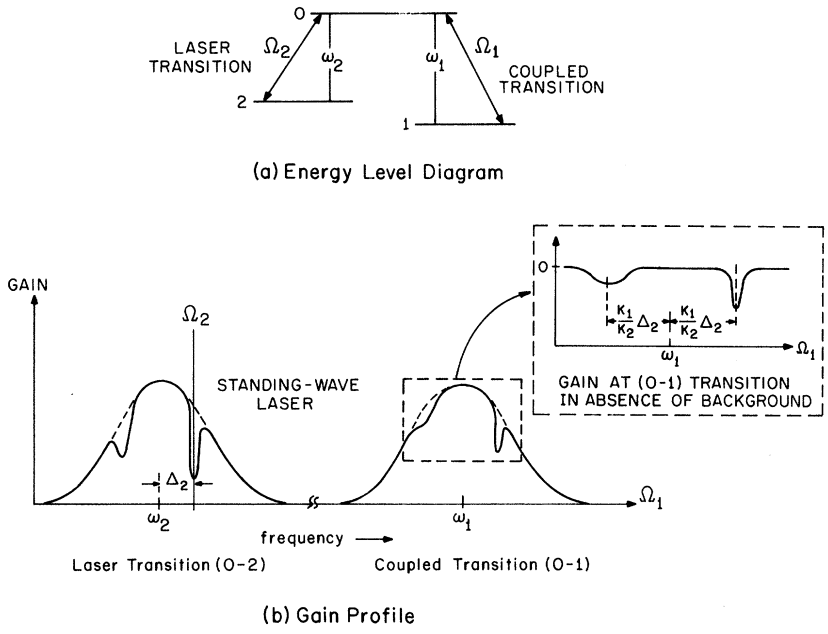

FIG. 1. (a) Energy-level scheme considered in this paper. Note that ω_1/ω_2 is variable and may be greater or less than unity. (b) Typical gain at Ω_1 for standing-wave field at Ω_2 detuned from resonance. The broad and narrow dips in the laser transition gain profile will be treated in a separate paper. The dips in the coupled transition are treated here. The insert depicts the dips as they occur in the absence of the background ($\langle R_{02}\rangle$ of the text). In the example shown, the background ($\langle R_{01}\rangle$) is unaltered by the standing-wave field. In other cases both terms may be influenced by it.

(or is weak). A detailed treatment was given in Ref. 4, the first paper in this series (which shall be referred to hereafter as I), using a method of calculation in which the EM fields are treated classically. The present paper extends this approach to the important case in which the laser is of arbitrary intensity and may be tuned to the center of its gain profile (conditions for Lamb dip). This case is of particular interest in view of the fact that recent theoretical studies[20,21] predict that under these conditions the laser-induced change in the velocity distribution departs from a simple Lorentzian-like curve. Instead, additional fine structure develops for atoms with low velocities[22] [Fig. 3(a)]. This fine structure does not manifest itself in the Lamb dip. We shall show below that related fine structure *does* appear in the gain profile of the coupled transition. This structure is particularly significant when the laser field is intense. An example is shown in Fig. 3(b), where the fine structure is clearly discernable on the wings of the central dip. The additional central feature of Fig. 3(a) results from other spatial interference effects to be described below.

When the laser field is intense other related line-shape effects can occur, even when the laser is detuned from the atomic center frequency. For example, when the laser frequency is higher than the frequency of the coupled transition under study, the narrow resonance splits in two (Fig. 4). This new effect should not be confused with another splitting effect which occurs for weak fields.[23-25] Both of these effects are treated below.

It should also be noted that the line-shape details analyzed here are of importance in considering stabilization schemes based on laser-induced line-narrowing effects.

This paper is divided into five sections. In Sec. II we set up the problem using the ensemble-averaged density-matrix equations of motion. We obtain an expression for the small-signal gain profile of a transition coupled to a laser transition, valid for arbitrary values of laser intensity, laser detuning, level lifetimes, Doppler width, and relative frequencies of laser and coupled transitions. These expressions are given in terms of continued frac-

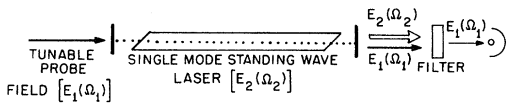

(a) Experimental Arrangement – Transmission

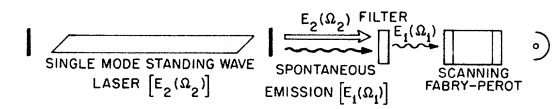

(b) Experimental Arrangement - Spontaneous Emission

FIG. 2. Possible experimental arrangements for observing laser-induced line narrowing. (a) Transmission: A tunable probe field $E_1(\Omega_1)$ is coaxial with standing-wave laser field $E_2(\Omega_2)$. A filter blocks E_2. The output intensity of the probe field is monitored as a function of Ω_1. (b) Spontaneous emission: The fluorescence spectrum $E_1(\Omega_1)$ emitted along the axis of the laser cavity is studied by means of a high-resolution scanning Fabry-Perot inteferometer. The filter transmits only E_1. The line-shape effects will be observed in both arrangements.

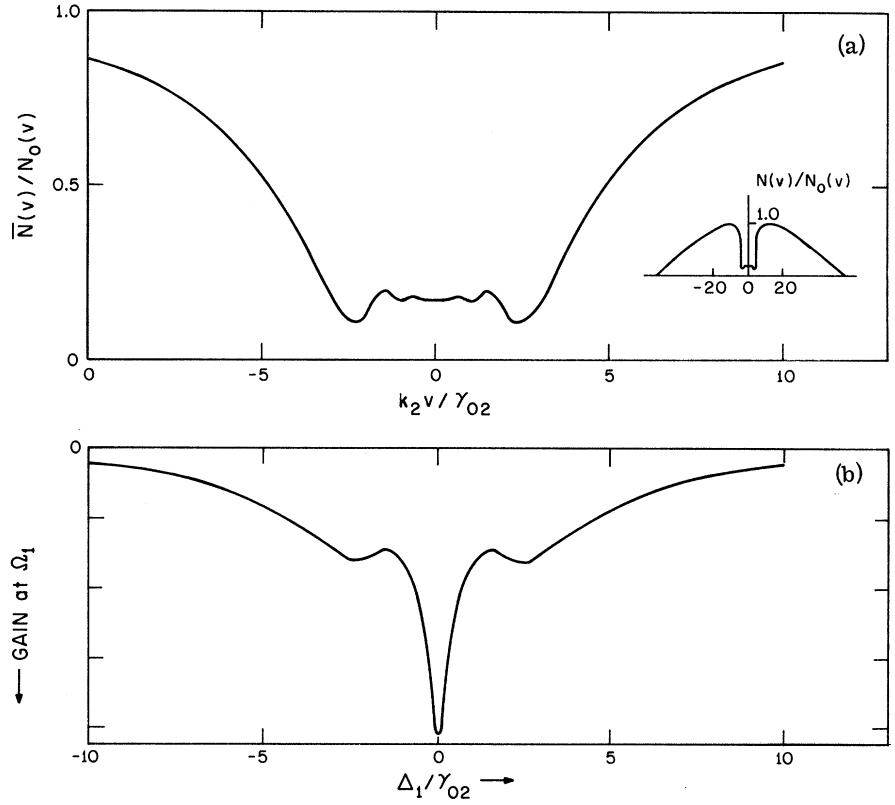

FIG. 3. (a) Plot of the spatially averaged population distribution vs axial velocity for the upper level of a two-level system interacting with an intense standing-wave field on resonance. Note the fine structure appearing in the central dip over a narrow range of velocities about $v = 0$. (b) Typical curve of gain at Ω_1 as a function of Δ_1, the detuning from the atomic center frequency of the coupled transition for the same case as Fig. 3(a). Comparison indicates that structure similar to the population fine structure occurs at the wings of the narrow central dip of the profile. The central dip itself originates from complex interference effects discussed in Sec. IV.

tions in the general case and Bessel functions in important special cases. In Sec. III computer methods of evaluating these expressions are discussed. In Sec. IV we present the results in a number of special cases which emphasize the different physical effects which come into play. These results are compared with a simplified expression obtainable from a rate-equation approximation, and also with the *independent-field approximation*. A brief discussion of the area (integrated intensity) properties of these results is given in Sec. V. Lengthy mathematical discussions which would interrupt the continuity are deferred to appendices.

II. THEORY

The theoretical problem under consideration is the interaction of a coupled Doppler-broadened three-level system with two coaxial applied fields, an intense standing-wave field resonating with the "laser" transition, and a weak traveling-wave probe field resonating with the coupled transition. To be concrete we shall deal with the folded level con-

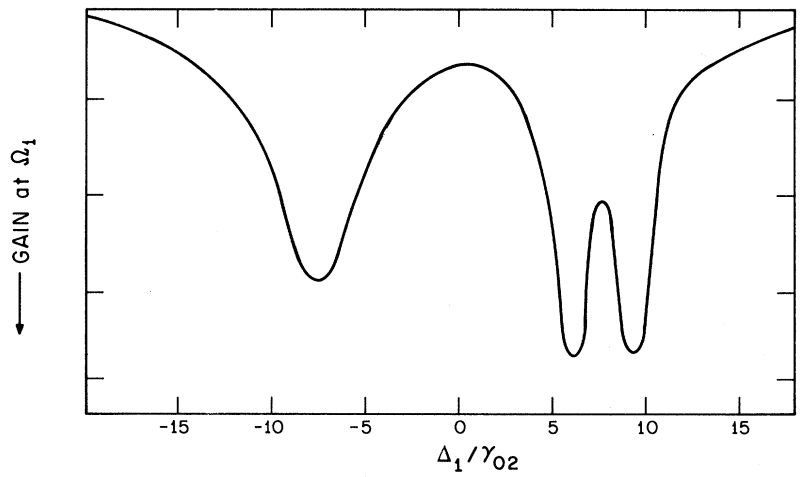

FIG. 4. Gain at Ω_1, background omitted, for the case $\omega_1 \simeq \omega_2/2$ as influenced by an intense standing-wave field E_2 detuned from resonance. Note that the dip on the right is split. For weakly saturating values of E_2, the splitting disappears. This new effect should not be confused with another effect which appears in the background term even for weakly saturating values of E_2 [see Fig. 7(d)].

figuration of Fig. 1(a). However, the results may be easily extended to the cascade configuration.[26]

In formulating the problem it is most convenient to treat the applied fields classically. It is important to note, however, that the resulting lineshape expression is also applicable to the case of spontaneous emission at the probe frequency.[27] The formalism of the ensemble-averaged density matrix is adopted. In this formalism one considers the interaction of the applied fields with atoms moving with a given axial velocity. Having obtained the response at the probe frequency, it is necessary to sum over the entire distribution of atomic velocities. Note that in the ensemble-averaged formalism the initial conditions at which individual atoms are produced have already been averaged over, a considerable simplification.

Consider, first, the interaction of the atoms in a narrow velocity band with the applied fields. The problem is solved by means of a perturbation technique. In the absence of the probe field the problem reduces to the interaction of a standing-wave field with a two-level system. We then consider the influence of the probe field as a small perturbation on this "unperturbed" system. The unperturbed problem has already been solved for arbitrary intensities and detuning of the standing-wave field in Ref. 21. Thus, we may directly substitute the required terms into the perturbation equations. In the unperturbed solution it is important to include spatial variations of high harmonic content produced by the standing-wave field in the level populations and the induced polarization, and in Ref. 21 the unperturbed solution is expressed as an infinite series of spatial Fourier components. In the present problem it is also convenient to expand the perturbation solution in spatial Fourier series. This immediately leads to an infinite set of coupled nonhomogeneous linear difference equations which may be solved subject to the appropriate boundary conditions. In the general case the solution may be expressed in terms of continued fractions and in important special cases in terms of Bessel functions. One then obtains an expression for the emission induced by the probe field due to atoms moving with one velocity. This expression is integrated over the atomic velocity distribution by means of computer to obtain the total emission due to atoms moving with all velocities. In some cases the integrations may be performed analytically.

The three-level system under study is of the type shown in Fig. 1(a). Level 0, the common level, is coupled to levels 1 and 2 by electric dipole matrix elements μ_{10} and μ_{20}, respectively. From parity considerations, $\mu_{21}=0$ and there are no diagonal matrix elements. Denote the energy of level j by $\hbar W_j$, and let $W_0 - W_j = \omega_j$; ω_1 and ω_2 fall in the optical-infrared region. The system interacts with a strong standing-wave laser field $E_2(z,t)$ at Ω_2, a frequency close to ω_2. The resonance at ω_1 is probed by the weak field $E_1(z,t)$ at variable frequency Ω_1. (We shall assume that $|\omega_2-\omega_1|$ is large compared to the Doppler widths so that E_1 does not resonate with ω_2, nor E_2 with ω_1.) Specifically,

$$E_1(z,\ t)=E_1^0\cos(\Omega_1 t - k_1 z+\phi_1)\ , \tag{1a}$$

$$E_2(z,\ t)=2E_2^0\ \sin k_2 z\ \cos(\Omega_2 t+\phi_2)\ , \tag{1b}$$

with

$$k_j=\Omega_j/c\ , \tag{1c}$$

and ϕ_1 and ϕ_2 are constant phase factors.[28] The additional condition

$$k_2=m\pi/L \tag{1d}$$

(L is the cavity length, m is an integer) is imposed on E_2 by the laser resonator. The total Hamiltonian for the system is

$$H=H_0+V\ , \tag{2}$$

where H_0 is the Hamiltonian of an unperturbed atom with stationary states of energy $\hbar W_j$, and V is the interaction Hamiltonian,

$$V=-\mu E(z,\ t)\ , \tag{3a}$$

$$E(z,\ t)=E_1(z,\ t)+E_2(z,\ t)\ , \tag{3b}$$

with electric dipole operator μ.

The problem is most readily treated by means of the ensemble-averaged density matrix $\rho(v,\ z,\ t)$, which describes an ensemble of atoms at coordinates $\{z,\ t\}$ moving with axial (z axis) velocity v. The equation of motion of ρ, derived in Ref. 21, is given by

$$\left(\frac{\partial}{\partial t}+v\ \frac{\partial}{\partial z}\right)\rho=-\frac{i}{\hbar}[H,\ \rho]-\tfrac{1}{2}\{\rho-\rho^0,\ \Gamma\}\ , \tag{4}$$

where [ ] and { } are commutator and anticommutator brackets, respectively. The left-hand side is the total derivative of ρ. Relaxation is accounted for in the second term on the right-hand side through Γ, which has elements

$$\Gamma_{ij}=\gamma_j\delta_{ij}\ , \tag{5}$$

where γ_j is the relaxation rate of level j. Also, ρ^0 describes the steady-state ensemble, assumed spatially uniform, in the absence of applied fields:

$$\rho^0_{ij}=n_j(v)\delta_{ij}\ , \tag{6}$$

$n_j(v)$ being the steady-state population density per velocity interval in level j in the absence of applied fields. We may write

$$n_j(v)=N_jG_j(v)\ , \tag{7a}$$

with N_j the total population density of level j and $G_j(v)$ its normalized velocity distribution:

$$\int_{-\infty}^{\infty} G_j(v)\,dv = 1 \,. \tag{7b}$$

For further details regarding Eq. (4) see Ref. 21.

The partial induced polarization due to the atoms moving with velocities in the interval between v and $v+dv$ is

$$P(v,\ z,\ t)dv = \mathrm{Tr}[\,\mu\rho\,]dv \,. \tag{8}$$

The net polarization is obtained by considering contributions from all velocities:

$$P(z,\ t) = \int_{-\infty}^{\infty} \mathrm{Tr}[\,\mu\rho]\,dv \,. \tag{9}$$

To formulate the perturbation approach, let us rewrite the Hamiltonian of Eq. (2) in the form

$$H = H^u + H' \,, \tag{10}$$

with

$$H^u = H_0 - \mu E_2 \tag{11}$$

and

$$H' = -\mu E_1 \,. \tag{12}$$

Thus, H^u is the unperturbed Hamiltonian, describing the interaction of the standing-wave field with the atomic system in the absence of E_1. The corresponding unperturbed density matrix ρ^u is the solution to Eq. (4) with H' equal to zero:

$$\left(\frac{\partial}{\partial t} + v\frac{\partial}{\partial z}\right)\rho^u = -\frac{i}{\hbar}[\,H^u,\ \rho^u\,] - \tfrac{1}{2}\{\rho^u - \rho^0,\ \Gamma\} \,. \tag{13}$$

The additional term H', due to the weak probe field, is taken to be a small perturbation on H^u. Thus, H' produces a small correction ρ' to ρ^u:

$$\rho = \rho^u + \rho' \,. \tag{14}$$

Inserting Eqs. (10) and (14) into Eq. (4), subtracting Eq. (13), and neglecting the $[H',\ \rho']$ term, which does not contribute to ρ' to lowest order in H', one obtains

$$\left(\frac{\partial}{\partial t} + v\frac{\partial}{\partial z}\right)\rho' = -\frac{i}{\hbar}[H',\ \rho^u] - \frac{i}{\hbar}[H^u,\ \rho'\,] - \tfrac{1}{2}\{\rho',\ \Gamma\} \,. \tag{15}$$

Assuming ρ^u is known, ρ' is completely specified by Eq. (15).

Equation (13) has been studied in detail in Ref. 21. Its solution, ρ^u valid for arbitrary values of E_2, has elements which can be written in the form

$$\rho^u_{20}(v,\ z,\ t) = \lambda^u(v,\ z)e^{i\Omega_2 t} \,, \tag{16a}$$

$$\lambda^u(v,\ z) = n_{02} \sum_{\text{odd } n \geq 1} [\,\Pi_n^+ e^{ink_2 z} + \Pi_n^- e^{-ink_2 z}\,] \,, \tag{16b}$$

$$\rho^u_{21} = \rho^u_{01} = 0 \,, \tag{16c}$$

$$\rho^u_{ik} = \rho^{u*}_{ki} \,, \tag{16d}$$

$$\rho^u_{00}(v,\ z,\ t) = n_0 + n_{02} \sum_{\text{even } n \geq 0} [\,a_n(v)e^{ink_2 z} + \text{c. c.}\,] \,, \tag{16e}$$

$$\rho^u_{22}(v,\ z,\ t) = n_2 + n_{02} \sum_{\text{even } n \geq 0} [\,b_n(v)e^{ink_2 z} + \text{c. c.}\,] \,. \tag{16f}$$

$$\rho^u_{11} = n_1 \,, \tag{16g}$$

where

$$n_{ij} = n_i - n_j \,. \tag{16h}$$

[In obtaining Eqs. (16) it is assumed, as stated above, that E_2 does not resonate with ω_1.] For convenience, a_n, b_n, and $\Pi_n^{\pm}$, obtained in Ref. 21, are given in Table I. Note that Z_n[Eq. (T14)] is a continued fraction which is to be evaluated subject to the boundary condition $Z_n \to 0$ for $n \to \infty$. The computation of Z_n is discussed in Sec. III.

Let us now consider Eq. (15). The weak probe field does not perturb the level populations, so that

$$\rho'_{kk} = 0, \quad k = 0,\ 1,\ 2. \tag{17}$$

Therefore, using Eqs. (16c) and (16g), the equations of motion of the off-diagonal matrix elements of ρ' may be written as

$$\left(\frac{\partial}{\partial t} + v\frac{\partial}{\partial z} + i\omega_1 + \gamma_{10}\right)\rho'_{01} = -\frac{i}{\hbar}[\,\mu_{01}E_1(\rho^u_{00} - n_1) - \mu_{02}E_2\rho'_{21}\,] \,, \tag{18a}$$

$$\left(\frac{\partial}{\partial t} + v\frac{\partial}{\partial z} + i(\omega_1 - \omega_2) + \gamma_{21}\right)\rho'_{21} = -\frac{i}{\hbar}[\,\mu_{01}E_1\rho^u_{20} - \mu_{20}E_2\rho'_{01}\,] \,, \tag{18b}$$

$$\left(\frac{\partial}{\partial t} + v\frac{\partial}{\partial z} - i\omega_2 + \gamma_{20}\right)\rho'_{20} = -\frac{i}{\hbar}[\,\mu_{20}E_2(\rho'_{22} - \rho'_{00}) + \mu_{10}E_1\rho^u_{21}\,] \,. \tag{18c}$$

This set of equations may be solved by inserting E_1 and E_2 [Eq. (1)] in complex form:

$$E_1(z,\ t) = A_1 e^{-ik_1 z}e^{i\Omega_1 t} + \text{c. c.}, \tag{19a}$$

$$E_2(z,\ t) = A_2(e^{ik_2 z} - e^{-ik_2 z})\,e^{i\Omega_2 t} + \text{c. c.} \,, \tag{19b}$$

with

$$A_1 = \tfrac{1}{2}E_1^0 e^{i\Phi_1} \,, \tag{20a}$$

$$A_2 = -\tfrac{1}{2}iE_2^0 e^{i\Phi_2} \,. \tag{20b}$$

The various spatial and temporal Fourier components of E_1 and E_2 drive the off-diagonal elements

TABLE I. Definition of symbols appearing in Eq. (16).

$$\gamma_{20}=\tfrac{1}{2}(\gamma_0+\gamma_2)\ , \tag{T1}$$

$$\Delta_2=\Omega_2-\omega_2\ , \tag{T2}$$

$$\beta=\frac{\mu_{02}E_2^0}{2\hbar}\,e^{-i\phi_2}\ , \tag{T3}$$

$$\beta_0=|\beta|\ , \tag{T4}$$

$$\bar{\gamma}=\gamma_0\gamma_2/\gamma_{20}, \tag{T5}$$

$$\Pi_n^+=-\frac{1}{2}\left[1-\frac{i\Delta_2}{\gamma_{20}+ink_2v}\right]\frac{\beta^*}{\beta_0}\,y_n\ , \tag{T6}$$

$$\Pi_n^-=\frac{1}{2}\left[1-\frac{i\Delta_2}{\gamma_{20}-ink_2v}\right]\frac{\beta^*}{\beta_0}\,y_n^*\ , \tag{T7}$$

$$\left.\begin{matrix}\Pi_n^+\\ \Pi_n^-\end{matrix}\right\}\ \text{odd}\ n\geq 1$$

$$a_n=\frac{1}{2}\left[\frac{\gamma_2+ink_2v}{\gamma_{20}+ink_2v}\right]\,y_n\ , \tag{T8}$$

$$b_n=-\frac{1}{2}\left[\frac{\gamma_0+ink_2v}{\gamma_{20}+ink_2v}\right]\,y_n\ , \tag{T9}$$

$$\left.\begin{matrix}a_n\\ b_n\end{matrix}\right\}\ \text{even}\ n\geq 2$$

$$a_0+a_0^*=(\gamma_2/2\gamma_{20})[y_0-1]\ , \tag{T10}$$

$$b_0+b_0^*=(-\gamma_0/2\gamma_{20})[y_0-1]\ . \tag{T11}$$

General expression for y_n:

$$y_0=\frac{1}{1+(4\beta_0/\bar{\gamma})\,\mathrm{Re}(Z_0)}\ , \tag{T12}$$

$$y_{n+1}=-Z_ny_n,\quad n=0,1,2,\ldots, \tag{T13}$$

$$Z_n=\cfrac{1}{F_{n+1}+\cfrac{1}{F_{n+2}+\cfrac{1}{F_{n+3}+\cdots}}}\ , \tag{T14}$$

with

$$\frac{1}{F_n}=\begin{cases}\beta_0[(\gamma_0+ink_2v)^{-1}+(\gamma_2+ink_2v)^{-1}]\ , & n=0,2,4,\ldots\\ \beta_0\{[\gamma_{20}+i(nk_2v+\Delta_2)]^{-1}+[\gamma_{20}+i(nk_2v-\Delta_2)]^{-1}\}, & n=1,3,5,\ldots\end{cases} \tag{T15}$$

evaluated subject to the condition

$$\lim_{n\to\infty}Z_n=0\ . \tag{T16}$$

Expression for y_n when $\gamma_0=\gamma_2\equiv\gamma$, $\Delta_2=0$:

$$y_n=\frac{i^nJ_{\nu(n)}(\eta)/J_{\nu(0)}(\eta)}{1+(4\beta_0/\gamma)\,\mathrm{Im}[J_{\nu(1)}(\eta)/J_{\nu(0)}(\eta)]}\ , \tag{T17}$$

$$\eta=4\beta_0/k_2v\ , \tag{T18}$$

$$\nu(n)=n-i\gamma/k_2v\ , \tag{T19}$$

with $J_\nu(z)$ equal to the Bessel function of order ν, argument z.

Rate-equation approximation to y_n:

$$y_0^{\mathrm{RE\,A}}=\frac{1}{1+(4\beta_0/\bar{\gamma})\,\mathrm{Re}(1/F_1)}\ , \tag{T20}$$

$$y_1^{\mathrm{RE\,A}}=-y_0^{\mathrm{RE\,A}}/F_1\ , \tag{T21}$$

$$y_n^{\mathrm{RE\,A}}=0,\quad n\geq 2\ . \tag{T22}$$

of ρ'. Let us consider the variations of the ρ'_{ij}. Of special importance are the coefficients of ρ'_{ij} on the left-hand sides of Eqs. (18). These are associated with the resonant behavior of the induced polarization. The only important frequency components of a ρ'_{ij} are those for which $\partial\rho'_{ij}/\partial t$ cancels the $i\omega$ factor for appropriate values Ω_1 and Ω_2, thereby reducing the coefficient of ρ'_{ij} to $\gamma_{ij}+v\partial/\partial z$. Therefore, a nearly complete solution to Eqs. (18) will be of the form

$$\rho'_{01}=\Lambda(v,\,z)\,e^{-i\Omega_1t}\ , \tag{21a}$$

$$\rho'_{21}=D(v,\,z)\,e^{i(\Omega_2-\Omega_1)t}\ , \tag{21b}$$

$$\rho'_{20}=\lambda(v,\,z)\,e^{i\Omega_2t}\ , \tag{21c}$$

where Λ, D and λ are time independent. Inserting Eqs. (16a), (19), and (21) into Eqs. (18) and equating like coefficients of the complex frequency factors, one finds that $\lambda(v,\,z)=0$ and that

$$\left(\Delta_1 + iv\,\frac{\partial}{\partial z} + i\gamma_{10}\right)\Lambda = \alpha^* e^{ik_1 z}(\rho_{00}^u - n_1) + i\beta(e^{ik_2 z} - e^{-ik_2 z})D\,, \tag{22a}$$

$$\left(\Delta_{12} + iv\,\frac{\partial}{\partial z} + i\gamma_{21}\right)D = \alpha^* e^{ik_1 z}\lambda^u + i\beta^*(e^{ik_2 z} - e^{-ik_2 z})\Lambda\,, \tag{22b}$$

where[28]

$$\alpha = \mu_{10}A_1/\hbar\,, \tag{23}$$

$$\beta = -i\mu_{02}A_2^*/\hbar\,, \tag{24}$$

$$\Delta_j = \Omega_j - \omega_j\,, \tag{25}$$

and

$$\Delta_{12} = \Delta_1 - \Delta_2\,. \tag{26}$$

We may proceed by expressing Λ and D in Fourier expansions in $k_2 z$. Note in Eq. (16) that ρ_{00}^u is expanded in the even harmonics of $k_2 z$, whereas λ^u is expanded in the odd harmonics. It directly follows from Eq. (22) that Λ will consist of the even harmonics of $k_2 z$, and D of the odd harmonics. Therefore, the required solution will be of the form

$$\Lambda(v, z) = \alpha^* e^{ik_1 z} \times\left(\Lambda_0 + \sum_{\text{even } n \geq 2}\left[\Lambda_n^+(v)\,e^{ink_2 z} + \Lambda_n^-(v)\,e^{-ink_2 z}\right]\right), \tag{27a}$$

$$D(v, z) = \alpha^* e^{ik_1 z}\sum_{\text{odd } n \geq 1}\left[D_n^+(v)\,e^{ink_2 z} + D_n^-(v)\,e^{-ink_2 z}\right]. \tag{27b}$$

The induced polarization at Ω_1, obtained from Eq. (8) and (21), is of the form

$$P_1(v, z, t) = \mathrm{Re}\left[2\mu_{10}\Lambda e^{-i\Omega_1 t}\right]. \tag{28}$$

The average power increase per unit volume at Ω_1 induced by E_1, due to atoms located at z and moving with axial velocity v, is given by

$$\Delta I(v, z)dv = -\langle \dot{P}_1(v, z, t)\,E_1(z, t)\rangle_{\text{time average}}\,dv\,. \tag{29}$$

The net power increase per unit volume is obtained by integrating this quantity over the distribution of atomic velocities and averaging it over the length l of the active medium, centered at position a:

$$\Delta I = (1/l)\int_{a-l/2}^{a+l/2} dz \int_{-\infty}^{\infty} dv\,\Delta I(v, z)\,. \tag{30}$$

Making use of Eqs. (29) and (27a), and indicating velocity averages by $\langle\ \rangle$, i.e., $\langle 0\rangle = \int_{-\infty}^{\infty} 0(v)\,dv$, we obtain

$$\Delta I = -2\hbar\Omega_1 \mid \alpha \mid^2 [\mathrm{Im}\langle\Lambda_0\rangle + \text{additional terms of the form } (\lambda/nl)\langle\Lambda_n^{\pm}\rangle], \tag{31}$$

where $\lambda = 2\pi/k_2$ is the wavelength of the intense standing-wave field. Since $\lambda/l \ll 1$, the additional terms are negligible as long as the $\Lambda_n^{\pm}$ do not diverge for large n. As shown in Appendix A, the convergence of the $\Lambda_n^{\pm}$ as $n \to \infty$ is a necessary condition for a physically acceptable solution. Accordingly, the additional terms may be neglected, and we obtain

$$\Delta I = -2\hbar\Omega_1 \mid \alpha \mid^2 \mathrm{Im}\langle\Lambda_0\rangle. \tag{32}$$

Note that only Λ_0 contributes to the net emitted power.

We now solve for Λ_0. Inserting Eqs. (16b), (16e), and (27) into Eqs. (22) and equating like harmonics of $k_2 z$, we obtain a set of equations which can be written in the following compact form:

$$\pm i\beta_0[x_{\pm}(n+1) - x_{\pm}(n-1)] + L(\pm n)x_{\pm}(n) = n_{02}t_{\pm}(n), \quad n \geq 1 \tag{33a}$$

$$i\beta_0[x_+(1) - x_-(1)] + L(0)x(0) = t(0)\,. \tag{33b}$$

The following definitions have been made:

$$x_{\pm}(n) = \begin{cases} (\beta/\beta_0)D_n^{\pm}\,, & n = 1, 3, 5, \ldots \quad (34a) \\ \Lambda_n^{\pm}\,, & n = 2, 4, 6, \ldots \quad (34b) \end{cases}$$

$$x_{\pm}(0) = x(0) = \Lambda_0\,, \tag{34c}$$

$$t_+(n) = \begin{cases} (\beta/\beta_0)\Pi_n^+\,, & n = 1, 3, 5, \ldots \quad (35a) \\ a_n\,, & n = 2, 4, 6, \ldots \quad (35b) \end{cases}$$

$$t_-(n) = \begin{cases} (\beta/\beta_0)\Pi_n^-\,, & n = 1, 3, 5, \ldots \quad (35c) \\ a_n^*\,, & n = 2, 4, 6, \ldots \quad (35d) \end{cases}$$

$$t(0) = n_{02}[a_0 + a_0^*] + n_{01}\,, \tag{35e}$$

$$L(\pm n) = \begin{cases} \Delta_{12} - (k_1 \pm nk_2)v + i\gamma_{21}\,, & n = 1, 3, 5, \ldots \quad (36a) \\ \Delta_1 - (k_1 \pm nk_2)v + i\gamma_{10}\,, & n = 0, 2, 4, 6, \ldots\,. \quad (36b) \end{cases}$$

Equations (33a) and (33b) constitute an infinite set of coupled nonhomogeneous linear difference equations, in which the $t_{\pm}(n)$'s, known quantities determined by the unperturbed solution, act as driving terms for the $x_{\pm}(n)$'s. We are particularly interested in obtaining Λ_0, since, from Eq. (32), the emitted power is proportional to $\mathrm{Im}\Lambda_0$. It is shown in Appendix A that the solution for Λ_0 is

$$\Lambda_0 = \frac{n_{01}+n_{02}\{a_0+a_0^*+\sum_{j=1}^{\infty}(-)^j[t_+(j)u_+(j)+t_-(j)u_-(j)]\}}{i\beta_0[u_+(1)-u_-(1)]+L(0)}, \tag{37}$$

where

$$u_\pm(j)=\prod_{k=1}^{j} W_\pm(k), \tag{38}$$

and $W_\pm(k)$ is the continued fraction

$$W_\pm(k)=\cfrac{\pm i\beta_0}{L[\pm k]}\Bigg/\left(1-\cfrac{\beta_0^2\,\frac{1}{L[\pm k]}\,\frac{1}{L[\pm(k+1)]}}{1-\cfrac{\beta_0^2\,\frac{1}{L[\pm(k+1)]}\,\frac{1}{L[\pm(k+2)]}}{1-\cdots}}\right) \tag{39a}$$

evaluated subject to the condition

$$\lim_{k\to\infty} W_\pm(k)=0\,. \tag{39b}$$

For the special case $\gamma_0=\gamma_2$, $\Delta_2=0$ we find

$$u_\pm(j)=\frac{i^j J_{\tau(j)}(-2\beta_0/k_2v)}{J_{\tau(0)}(-2\beta_0/k_2v)}\,, \tag{40a}$$

$$\tau(j)=\mp L(\pm j)/k_2v\,, \tag{40b}$$

where $J_\tau(z)$ represents a Bessel function of complex order τ and (real) argument z. The final expression for ΔI may be obtained from Eqs. (32), (37), and (38). The numerical evaluation of $W_\pm(k)$ is discussed in Sec. III.

III. COMPUTER EVALUATION OF ΔI

The calculation of ΔI, the emitted power at Ω_1, from Eqs. (35), (37)–(39), and (32), requires the evaluation of continued fractions and velocity integrals. The computations have been performed on the MIT 360 computer using double-precision complex arithmetic. Continued fractions were evaluated by comparing the value obtained by truncating the continued fraction after j terms with the value obtained by truncating after $j+1$ terms. The algorithm used in calculating a truncated continued fraction of j terms is given in Appendix C. If the absolute value of the fractional difference between the two calculated values is less than 10^{-6}, the $j+1$th value is taken as the numerical answer. The $u_\pm$'s and y's represented as convergent continued fractions have been calculated from Eqs. (38) and Table I with all the continued fractions computed independently to ensure that small errors did not propagate. In the summations in Eqs. (37) sufficient terms were included so that the absolute value of the ratio of the last value to the first is less than 10^{-6}. The convergence of this sum is a consequence of the boundary conditions, which require Λ_n to approach 0 for large n (Appendix A).

As a check, when $\gamma_0=\gamma_2$ and $\Delta_2=\Delta_1$ we have compared our continued-fraction results with the Bessel function expressions and find agreement to six places of accuracy.

To simplify the interpretation of our results, we have chosen a rectangular population distribution,

$$G_j(v)=\begin{cases} k_2/69.8\gamma_{20} & \text{for } |v| \le 34.9\gamma_{20}/k_2 \\ 0 & \text{for } |v| > 34.9\gamma_{20}/k_2 \end{cases}$$

for all values of j. This wide distribution leads to intensity profiles in which effects due to finite velocity distribution are greatly reduced.[29] It would, of course, be easy to insert any desired form of $G_j(v)$ into the program.

The velocity integrations are evaluated using Simpson's rule with intervals of $0.2k_2v/\gamma_{20}$. The accuracy of the integration is better than 2%. The accuracy of our calculations was checked by decreasing the step size and increasing the limits of integration. Our numerical results are in excellent agreement with the limiting case of a weakly saturating standing-wave field (third-order polarization) and with the case in which the laser is of arbitrary intensity but significantly detuned, cases for which we have obtained analytic expressions (see discussion below).

IV. RESULTS

Equation (32) may be written in the following form:

$$\Delta I(\Omega_1)=\hbar\Omega_1\langle (n_2-n_1)J_{21}+(n_0-n_1)J_{01}\rangle \tag{41}$$

(as before, $\langle\ \rangle$ indicates velocity average), where

$$J_{21}=2\,|\,\alpha\,|^2 \times \mathrm{Im}\,\frac{a_0+a_0^*+\sum_{j=1}^{\infty}(-1)^j[t_+(j)u_+(j)+t_-(j)u_-(j)]}{i\beta_0[u_+(1)-u_-(1)]+L(0)}\,, \tag{42a}$$

$$J_{01}=-2\,|\,\alpha\,|^2 \times \mathrm{Im}\,\frac{1+a_0+a_0^*+\sum_{j=1}^{\infty}(-1)^j[t_+(j)u_+(j)+t_-(j)u_-(j)]}{i\beta_0[u_+(1)-u_-(1)]+L(0)}\,. \tag{42b}$$

Expressions in the same form for the off-resonance case $\Delta_2/\gamma_{20} > (1+\frac{1}{2}I)^{1/2}$ were previously discussed in Paper I, where it was shown that J_{21} represents the *double-quantum* transition rate per atom, in which atoms produced in level 2 subsequently decay from level 1 by the net exchange of two photons with the applied radiation fields, one absorbed at

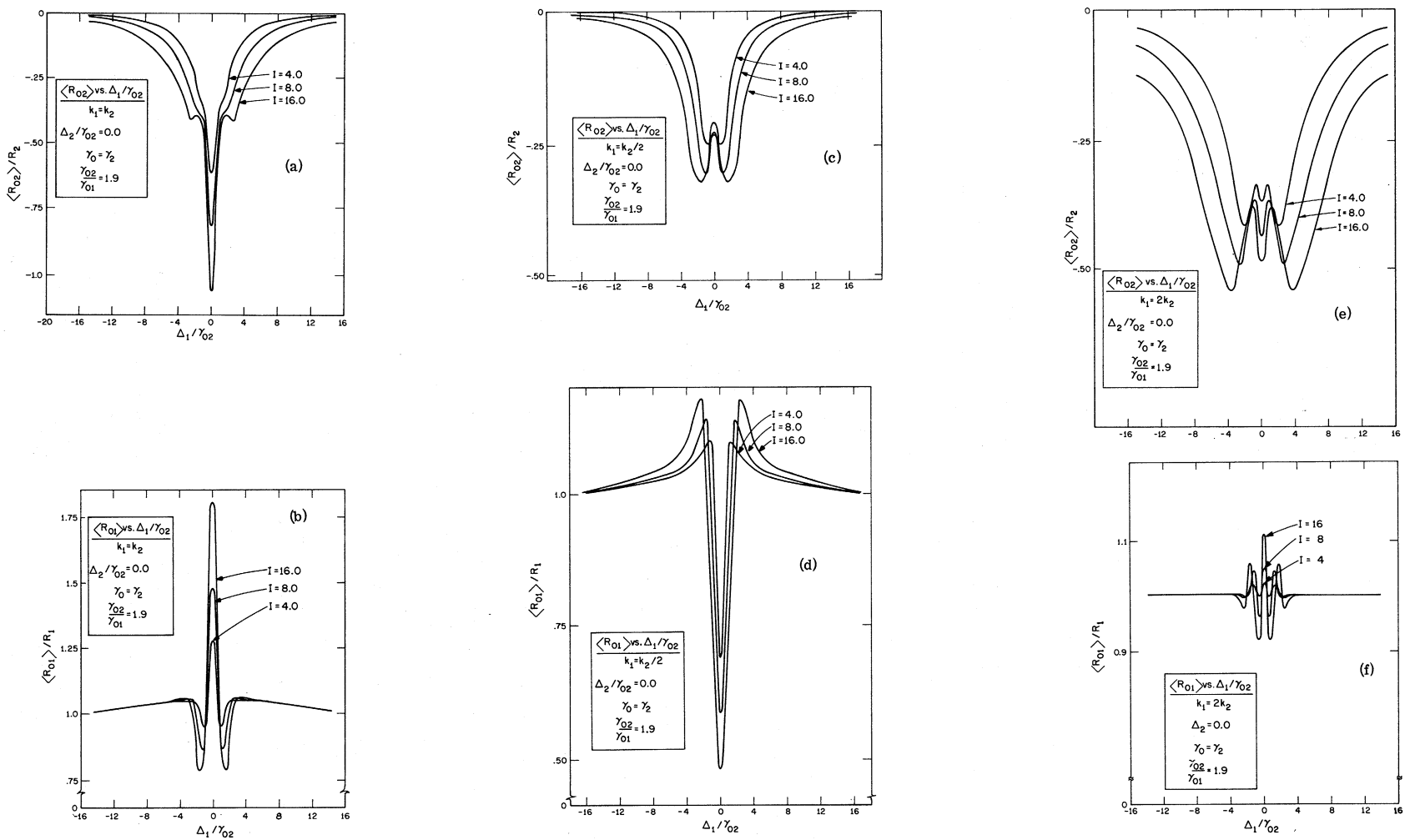

FIG. 5. Intense standing-wave field on resonance ($\Delta_2 = 0$). (a) $\langle R_{02} \rangle$ vs Δ_1 for $k_1 = k_2$. The additional structure on the sides of the central dip emerges as I increases. The latter structure is closely correlated with the structure in the space-averaged population distribution [Fig. 3(a)]. (b) $\langle R_{01} \rangle$ vs Δ_1 for the same conditions as in (a). Note that this structure would be present even if the medium were transparent ($n_2 = n_0$). (c) $\langle R_{02} \rangle$ vs Δ_1 for $k_1 = \frac{1}{2}k_2$. The splitting observed in the central dip also occurs when E_2 is off resonance [Fig. 6(c)] and is a traveling-wave effect. (d) $\langle R_{01} \rangle$ vs Δ_1 for the same conditions as in (c). This structure also occurs in the detuned case [Fig. 6(d)] and is a traveling-wave effect. (e) $\langle R_{02} \rangle$ vs Δ_1 for $k_1 = 2k_2$. The complex structure observed within the broad central dip is the result of interference effects due to the standing-wave nature of E_2 and does not appear when E_2 is detuned [Fig. 6(e)]. (f) $\langle R_{01} \rangle$ vs Δ_1 for the same conditions as in (e). The structure here is also the result of standing-wave interference effects and does not appear when E_2 is detuned [Fig. 6(f)].

Ω_2 and one emitted at Ω_1. J_{01} was introduced as the *single-quantum* transition rate per atom, due to atoms produced in level 0 which subsequently decay from level 1, emitting a single photon at Ω_1. In this paper, however, we find it more convenient to express our results for $\Delta I(\Omega_1)$ in terms of $n_0 - n_2$ and $n_0 - n_1$. We thus have, equivalent to Eq. (41),

$$\Delta I(\Omega_1) = \hbar\Omega_1 [\langle R_{02}\rangle + \langle R_{01}\rangle] , \tag{43a}$$

where

$$R_{02} = -2n_{02} |\alpha|^2 \times \mathrm{Im} \frac{a_0 + a_0^* + \sum_{j=1}^{\infty} (-1)^j [t_+(j)u_+(j) + t_-(j)u_-(j)]}{i\beta_0 [u_+(1) - u_-(1)] + L(0)} , \tag{43b}$$

$$R_{01} = -2n_{01} |\alpha|^2 \mathrm{Im}\{i\beta_0 [u_+(1) - u_-(1)] + L(0)\}^{-1} . \tag{43c}$$

In Figs. 5–8, $\langle R_{02}\rangle$ and $\langle R_{01}\rangle$ are plotted for various parameters. For convenience we have introduced the usual saturation parameter

$$I = 8\beta_0^2/\gamma_0\gamma_2 \tag{44}$$

as a measure of the intensity of the standing-wave field (E_2). In Figs. 5, 7(a), and 7(b) the standing-wave field is on resonance ($\Delta_2/\gamma_{02} = 0$). In Figs. 6, 7(c), and 7(d) the standing-wave field is off resonance [$\Delta_2/\gamma_{02} \gg (1 + \frac{1}{2}I)^{1/2}$]. In Figs. 8(a) and 8(b) the standing-wave field is near resonance [$\Delta_2/\gamma_{02} \approx (1 + \frac{1}{2}I)^{1/2}$].

Briefly, the general behavior of the curves is as follows.

$\langle R_{02}\rangle$ *curves.* When the laser is detuned a pair of resonances, one broad, one narrow, but of equal area, occurs symmetrically located about ω_1. In the folded configuration discussed here [Fig. 1(a)] the narrow resonance and the laser are always detuned to the same side of their respective Doppler profiles. [In a cascade configuration the positions of narrow and broad resonances would be interchanged (Paper I).] When $k_2 > k_1$ the narrow resonance splits into two for intense laser fields. As the laser is tuned to line center the resonances overlap and additional complex structure develops.

$\langle R_{01}\rangle$ *curves (background).* The background is unaffected by the laser when detuned, except in the case $k_2 > k_1$, in which structure develops on the same side of the Doppler profile as the narrow resonance in the $\langle R_{02}\rangle$ curves. (In no case does structure occur on the opposite side of the Doppler profile.) As the laser is tuned to line center, structure emerges for all values of k_1/k_2. This structure becomes more pronounced as the laser intensity increases. In every case the area under the background curve is unchanged by the presence of the laser field.

The additional features occurring on resonance are due to the standing-wave nature of the intense field, whose oppositely propagating traveling-wave components simultaneously interact with atoms moving in the same narrow range of velocities. Off resonance, where the traveling-wave components of E_2 no longer couple to the same atomic velocity band, the line shapes can be analyzed in terms of the two oppositely directed traveling waves at Ω_2 which do not couple to one another. It will be shown below that in the detuned case the line shape expressions considerably simplify and can be written in closed algebraic form.

A. Intense Standing-Wave Field: On Resonance ($\Delta_2 = 0$)

Typical results obtained from Eqs. (43) are shown in Figs. 5(a)–5(f). Some of the line-shape effects of Figs. 5 are traveling-wave effects and also occur when the laser field is detuned. Others are inherently standing wave in nature and do not occur in the detuned case. To gain some understanding of the latter class of effects, let us consider the on-resonance and detuned line-shape curves for the special case $k_1 = k_2$ [Figs. 5(a) and 5(b), and Figs. 6(a) and 6(b), respectively].

When the laser field $E_2(z, t)$ is in the form of a traveling wave, only a single resonance occurs on the $\langle R_{02}\rangle$ curve, narrow if E_2 is parallel to E_1, broad if E_2 is antiparallel to E_1. The $\langle R_{01}\rangle$ background curve is unaltered by the field. No additional structure appears as E_2 is tuned through resonance. (A detailed discussion of the narrow and broad resonances in the traveling-wave case is given in Paper I.)

Next, consider the case in which $E_2(z, t)$ is in the form of a standing wave. This field may be decomposed into two traveling-wave components of equal amplitudes propagating in opposite directions. Let us denote the component of E_2 propagating in the $\pm z$ direction by $E_2^{\pm}$. Note that E_1 also propagates in the $+z$ direction. To a group of atoms traveling with axial velocity v, the frequency of $E_2^{\pm}$ appears Doppler-shifted to $\Omega_2 \mp k_2 v$. Since $E_2^{\pm}$ resonantly couples to atoms for which $\omega_2 = \Omega_2 \mp k_2 v$, if E_2 is detuned from ω_2, E_2^+ and E_2^- resonate with atoms in different velocity bands. In other words, E_2^+ and E_2^- act independently. Accordingly, when E_2 is detuned from ω_2, then E_2 and E_2 resonate with atoms in the broad and narrow traveling-wave resonances, well resolved from each other and symmetrically located about ω_1 [Fig. 6(a)]. As before, the $\langle R_{01}\rangle$ curve shows no structure [Fig. 6(b)].

As the laser is tuned to line center the $\langle R_{02}\rangle$ resonances merge, but the resulting curve is *not* a simple superposition of broad and narrow signals: Additional complex structure occurs [Fig. 5(a)]. Now, for the first time, the $\langle R_{01}\rangle$ curve also ex-

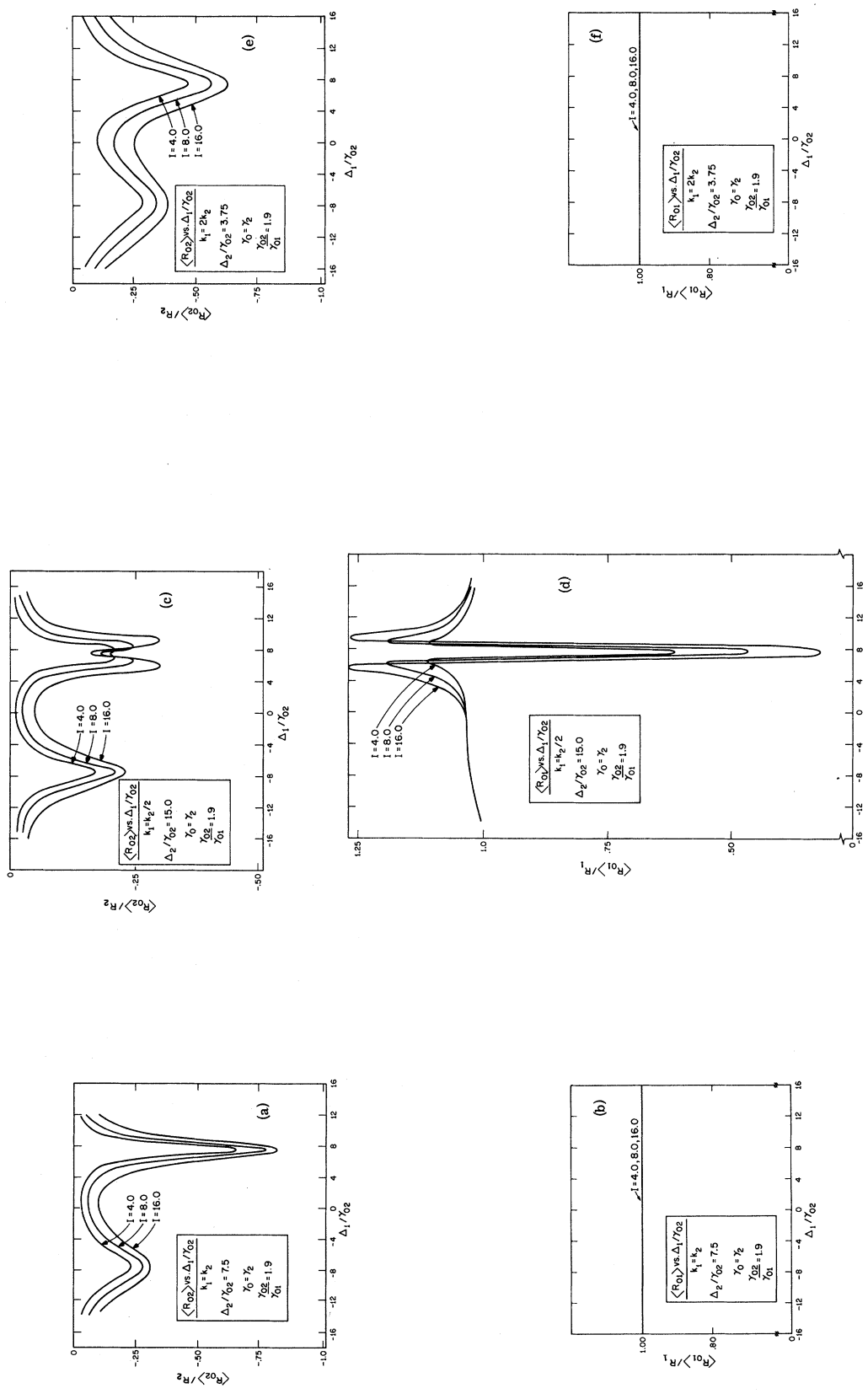

FIG. 6. Intense standing-wave field well detuned from resonance ($\Delta_2/\gamma_{02} = 7.5k_2/k_1$). (a) $\langle R_{02}\rangle$ vs Δ_1 for $k_1 = k_2$. Two Lorentzian resonances occur at $\Omega_\pm = 0$ of full width at half-maximum (FWHM) $\Gamma_\pm$, respectively, in accord with the analytic expressions (50c). (b) $\langle R_{01}\rangle$ vs Δ_1 for same conditions as in (a). Note that E_2 has negligible effect on the background. (c) $\langle R_{02}\rangle$ vs Δ_1 for $k_1 = \frac{1}{2}k_2$. A Lorentzian of width Γ_- occurs at $\Omega_- = 0$. The resonance at $\Omega_+ = 0$ splits in two, with increasing splitting for increasing values of I. (d) $\langle R_{01}\rangle$ vs Δ_1 for the same conditions as (c). The background curve exhibits non-Lorentzian structure at $\Omega_+ = 0$. No structure appears at $\Omega_- = 0$. (e) $\langle R_{02}\rangle$ vs Δ_1 for $k_1 = 2k_2$. Lorentzian resonances of widths $\Gamma_\pm$ occur at $\Omega_\pm = 0$. (f) $\langle R_{01}\rangle$ vs Δ_1 for the same conditions as in (e). The flat curve indicates that E_2 has a negligible effect on $\langle R_{01}\rangle$ when the standing-wave field is detuned.

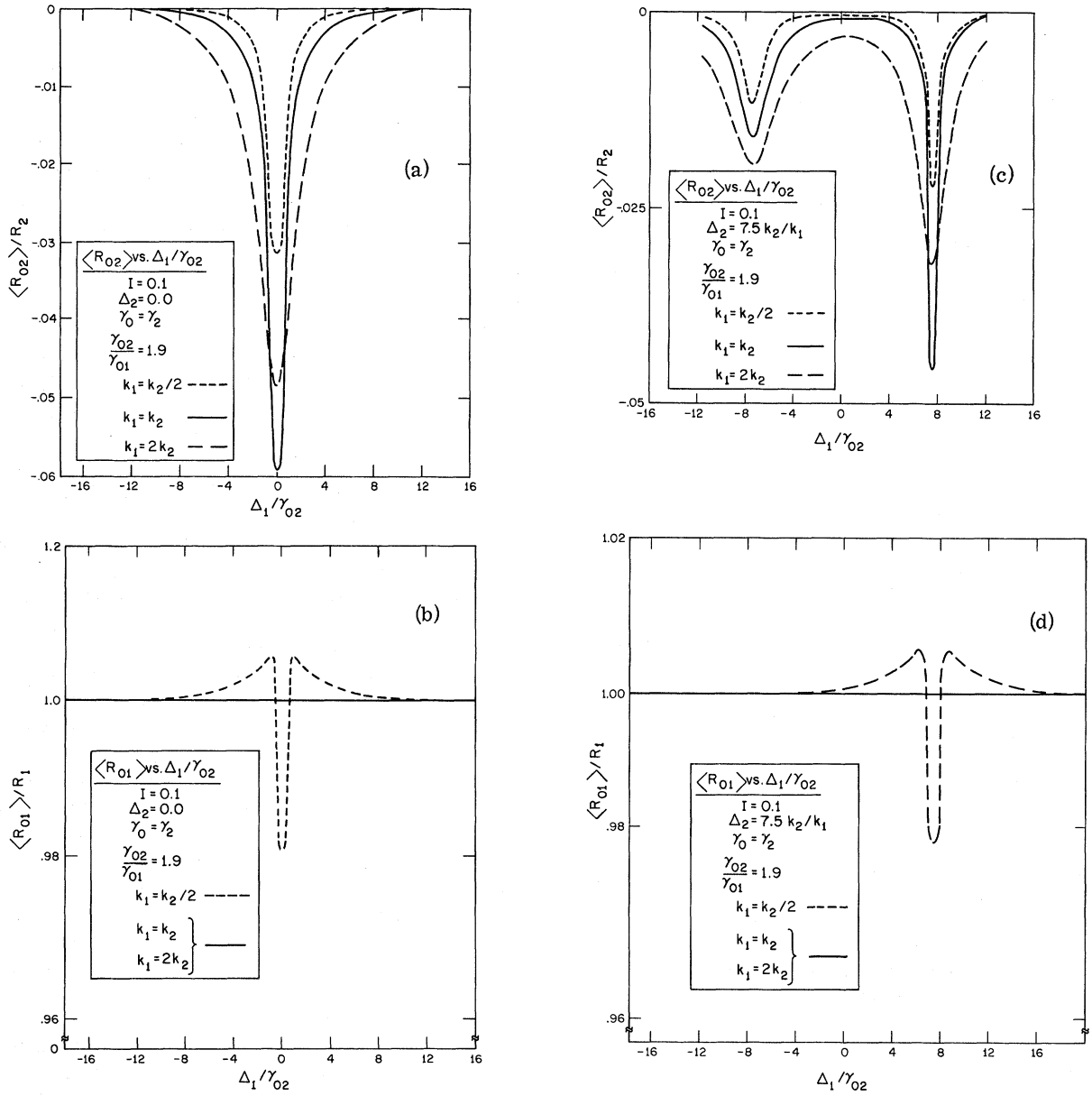

FIG. 7. Weakly saturating standing-wave field. (a) $\langle R_{02}\rangle$ vs Δ_1 for $\Delta_2 = 0$. In the weak-field limit the resonances at $\Delta_1 = 0$ are essentially the sum of two Lorentzians of widths Γ_+ and Γ_-. (b) $\langle R_{01}\rangle$ vs Δ_1 for $\Delta_2 = 0$. Note that for $k_1 \geq k_2$, the background curve is unaffected by E_2. However, for $k_1 < k_2$, a non-Lorentzian structure appears about $\Delta_1 \cong 0$. (c) $\langle R_{02}\rangle$ vs Δ_1 for $\Delta_2 = 7.5\,k_2/k_1$. The two resonances at $\Omega_\pm = 0$ are of widths $\Gamma_\pm$. (d) $\langle R_{01}\rangle$ vs Δ_1 for $\Delta_2 = 7.5\,k_2/k_1$. These curves are the same as the background curves of (b) except that the non-Lorentzian resonance at $\Omega_+ = 0$ in the $k_1 = \frac{1}{2}k_2$ curve is shifted.

hibits structure [Fig. 5(b)]. These new features arise because at line center E_2^+ and E_2^- resonante with the same velocity band of atoms (in the vicinty of $v = 0$). Thus, viewed in the atoms' rest frame, the response at Ω_1 is due to the simultaneous interaction of three fields, E_2^+, E_2^-, and E_1. The coupling of E_2^+, at frequency $\Omega_2 - k_2 v$, and E_2^-, at $\Omega_2 + k_2 v$, produces sidebands in the atomic response at harmonics of $k_2 v$—viewed in the rest frame of the moving atoms. Note that in the laboratory frame a time variation of the type $(\Omega_2 - nk_2 v)t$ will appear as the space-time variation $\Omega_2 t - k_2 z$, since $z = vt$.[21] Thus, in Eq. (16) it can be seen that the unperturbed density matrix elements ρ_{00}^u, ρ_{22}^u, and ρ_{20}^u all contain harmonics of $k_2 z$. The resulting induced polarization at Ω_1 [which is proportional to $\Lambda(v, z)$] is driven by both ρ_{00}^u and ρ_{20}^u [Eqs. (22)]. In addition, the ρ_{21}' term, which is due to coherent transitions between

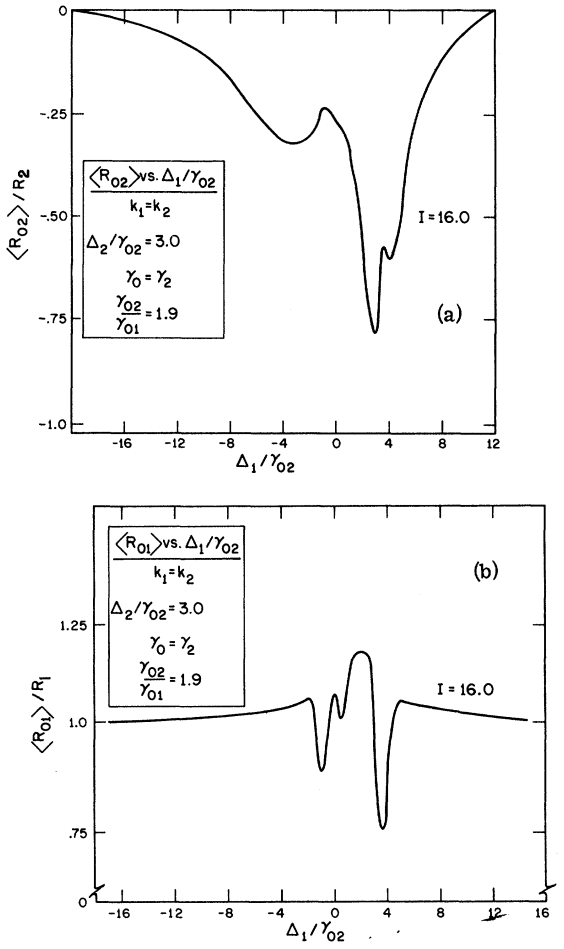

FIG. 8. Plots of $\langle R_{02}\rangle$ (a) and $\langle R_{01}\rangle$ (b) vs Δ_1 for $I=16$, $k_1=k_2$, for the case in which E_2 is near resonance, $\Delta_2/\gamma_{02}=3.0$. These curves show features common to both the off-resonance and on-resonance conditions, indicating the complexity of the line shape resulting from the interference effects treated in this paper.

levels 2 and 0 and level 1, also contains harmonics of $k_2 z$, even in the absence of the driving terms. Note that ρ'_{21} also contributes to $\Lambda(v,z)$. Therefore, the induced polarization at Ω_1 contains components modulated at spatial harmonics of $k_2 z$. The on-resonance inherently standing-wave line-shape features are thus seen to be due to spatial interference effects. It should be pointed out that although the final intensity expressions depend directly only on Λ_0, the dc spatial fourier component of $\Lambda(v,z)$, high spatial harmonics considerably influence the form of Λ_0 through the recurrence relations, Eqs. (33). Indeed, if these spatial interference effects are neglected the complex structure does not appear. This limit, known as the "rate-equation approximation," is discussed below.

The structure in the $\langle R_{02}\rangle$ line shape is due to spatial variations which enter through the unperturbed terms ρ^u_{20} and ρ^u_{00}, and also through the interference term ρ'_{21}, which is due to the direct nonlinear interaction of E_1 and E_2 occurring even in the absence of a population difference between levels 0 and 2. In contrast, the structure on the $\langle R_{01}\rangle$ background line shape is exclusively due to the ρ'_{21} term. Hence the characteristic behavior of the background term is distinct from that of the $\langle R_{02}\rangle$ term. Note that background structure can occur even when there is complete transparency at the laser transition ($n_2=n_0$). It is also interesting to note that the area under the background curves remains unaffected by the laser field in all cases, a consequence of the fact that the area of the response of *each* atomic velocity ensemble is unaltered by the laser field. A comprehensive discussion of this fact will be presented in a forthcoming paper.

It is worthwhile to reexamine the above line-shape features from another point of view. In Refs. 20 and 21 it was shown that when an intense standing-wave field is tuned to the center of the Doppler profile of a two-level system, fine structure occurs in the *spatially averaged population distribution.* An example is shown in Fig. 3(a). This structure results from the coherent ringing of slow atoms moving through the spatial nodes of the standing-wave field (see Ref. 21, Sec. 7 for detailed discussion). This curve is compared with a corresponding $\langle R_{20}\rangle$ curve, Fig. 3(b). The influence of the deformations in the spatially averaged velocity distribution is clearly evident on the wings of the central dip. No such fine structure appears in the central tuning dip of the two-level *gain profile* (or the Lamb dip), obtained by tuning the intense field through the center of the atomic resonance. Thus experimental observation of curves such as $\langle R_{02}\rangle$ of Fig. 3(b) would not only confirm the present results but would also provide evidence of the population structure predicted in Refs. 20 and 21.

Indeed, a major incentive of this work has been to determine the extent to which the structure in the population distribution would manifest itself in the radiation at the coupled transition.

This behavior was anticipated on the basis of a simple argument ignoring field interactions between E_1 and E_2, the "independent-field approximation" (IFA). In this limit the spontaneous emission per unit frequency interval at Ω_1 is given by

$$\Delta I(\Omega_1)_{\mathrm{IFA}} = \hbar\Omega_1 \frac{\gamma_0\gamma_{10}}{\pi} \left\langle \frac{|(n_0+n_{02}[a_0+a_0^*])}{(\Delta_1-k_1v)^2+\gamma_{10}^2} \right\rangle , \tag{45}$$

where $n_0+n_{02}(a_0+a_0^*)$ is the spatially uniform component of $\rho^u_{00}(v)$, Eq. (16e), in the presence of the standing-wave laser field. One would expect the fine structure to wash out for $\gamma_{10}\gg\gamma_{20}$ since in this case the broad Lorentzian cannot follow the narrow structure within the population curve (whose fine

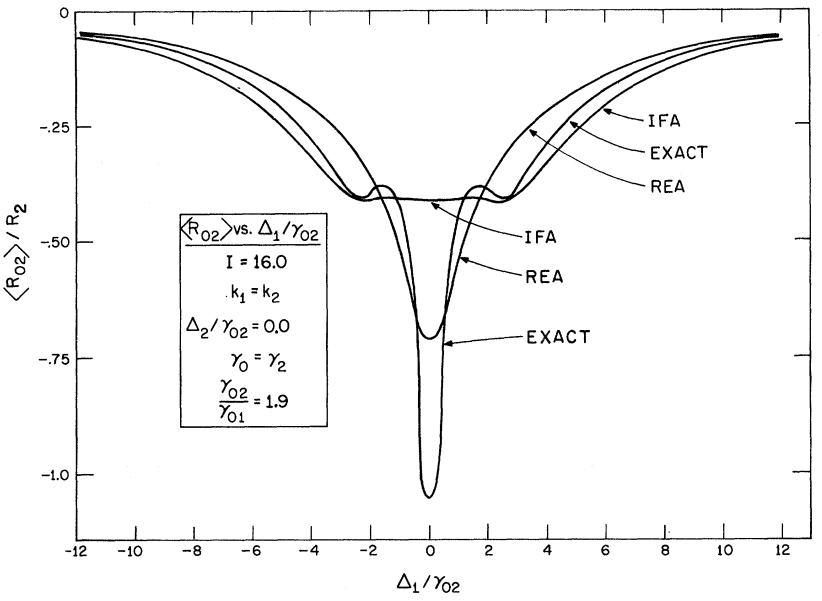

FIG. 9. Comparison of $\langle R_{02}\rangle$ vs Δ_1 for $I=16$, $k_1=k_2$ for the exact solution [Eq. (43b)], the IFA [Eq. (45)], and the REA [Eq. (A23)]. Note that structure in the exact curve on the wings of the central dip coincides with the residual structure in the IFA arising because of the fine structure in the population distribution of level 2, although the structure in the exact curve is significantly enhanced. This enhancement results from spatial interference effects and does not appear in the REA curve. The narrow central dip in the exact curve is in part due to the field interactions between E_1 and E_2 in the absence of spatial variations in the population of level 2, as can be seen by comparison with the central dip of the REA curve. The exact curve, however, is further influenced by spatial interference effects.

structure is of the order of γ_{20}). However, with $\gamma_{10}\lesssim\gamma_{20}$ fine structure would occur. Needless to say, the IFA expression is not rigorous, and the IFA does not predict the deep central dip obtained from the exact expression. For purposes of comparison the IFA results are plotted together with the exact expression for $\langle R_{02}\rangle$ [Eq. (43b)] and the corresponding rate-equation approximation (REA), discussed below, in Fig. 9.

For the case $k_1\neq k_2$ additional line-shape features develop. These features are also observed when the laser is detuned from resonance, where they can be separated from the standing-wave interactions discussed above. We turn now to a discussion of these traveling-wave effects, which can be given in terms of simplified expressions for $\langle R_{02}\rangle$ and $\langle R_{01}\rangle$, valid for a detuned standing-wave laser field of arbitrary intensity.

B. Intense Standing-Wave Field: Off Resonance $[\Delta_2/\gamma_{20}\gg(1+\frac{1}{2}I)^{1/2}]$

Next consider the case when the laser field is detuned [Figs. 6, 7(c), and 7(d)]. In this limit, R_{02} and R_{01} reduce to

$$R_{02}=-n_{02}\beta_0\,|\,\alpha\,|^2 \times \mathrm{Im}\,\frac{\dfrac{y_1^{\mathrm{REA}}}{L(1)}\left[\dfrac{\Delta_2}{\gamma_{02}+ik_2v}+\dfrac{2L(1)+i\gamma_0}{\gamma_0}\right]+\dfrac{y_1^{\mathrm{REA}*}}{L(-1)}\left[\dfrac{\Delta_2}{\gamma_{02}-ik_2v}+\dfrac{2L(-1)+i\gamma_0}{\gamma_0}\right]}{-\beta_0^2[1/L(1)+1/L(-1)]+L(0)}, \tag{46a}$$

$$R_{01}=-2n_{01}\,|\,\alpha\,|^2\,\mathrm{Im}\{-\beta_0^2[1/L(1)+1/L(-1)]+L(0)\}^{-1}, \tag{46b}$$

where y_1^{REA} is given in Table I, Eq. (T21). These results are equivalent to the REA, in which the spatial harmonics induced by the standing-wave field are neglected (see Appendix A and Table I). Since we are restricting our considerations here to the detuned case, Eqs. (46) further simplify to

$$R_{02}=R_{02}(+)+R_{02}(-), \tag{47a}$$

$$R_{01}=R_{01}^0+R_{01}(+)+R_{01}(-), \tag{47b}$$

with

$$R_{02}(\pm)=4n_{02}\,|\,\alpha\,|^2\beta_0^2 \times \mathrm{Im}\,\frac{\gamma_0^{-1}\,\mathrm{Re}(1/F_\mp)+i/[2L(\mp1)F_\mp]}{[1+(4\beta_0^2/\bar\gamma)\,\mathrm{Re}(1/F_\mp)][L(0)-\beta_0^2/L(\mp1)]}$$

$$=-2n_{02}\,|\,\alpha\,|^2\beta_0^2 \times \mathrm{Im}\,\frac{2(\gamma_{20}/\gamma_0)\,L(\mp1)+iF_\mp^*}{[\,|F_\mp|^2+4(\gamma_{20}/\bar\gamma)\,\beta_0^2][-L(\mp1)\,L(0)+\beta_0^2]}, \tag{48a}$$

where

$$F_\pm=\gamma_{20}+i(\Delta_2\pm k_2v), \tag{48b}$$

and

$$R_{01}(\pm) = -2n_{01} \mid \alpha \mid^2 \beta_0^2 \ \mathrm{Im} \frac{1}{L(0)[L(0)L(\mp 1) - \beta_0^2]} , \tag{49a}$$

$$R_{01}^0 = -2n_{01} \mid \alpha \mid^2 \mathrm{Im}[1/L(0)] . \tag{49b}$$

The terms naturally break into pairs (+ and −) as a consequence of the fact, discussed above, that when E_2 is detuned from resonance, its oppositely directed traveling-wave components, E_2^+ and E_2^-, couple to distinct bands of atoms moving with opposite velocities. In fact, the $R_{0j}(\pm)$ line-shape expression is due to $E_2^\pm$ interacting with E_1. (Recall that E_2^+ propagates parallel to E_1, whereas E_2^- propagates antiparallel to E_1.) Note that R_{01}^0 represents the usual background term in the absence of E_2. These results were previously obtained in Paper I [cf. Eqs. (I33) and (I34)], where the intense field was assumed to be in the form of a traveling wave.

In the Doppler-broadened limit the velocity integration of Eqs. (48) and (49) may be carried out analytically.[30] The results for the two cases $k_1 > k_2$ and $k_1 < k_2$ differ qualitatively.

Case 1. $k_1 \geq k_2$. In this case we find that

$$\langle R_{01}^0 \rangle = R_1 W_{01}(\Delta_1/k_1) , \tag{50a}$$

$$\langle R_{01}(\pm) \rangle = 0, \tag{50b}$$

$$\langle R_{02}(\pm) \rangle = R_2 W_{02}(\Delta_1/k_1) \frac{2k_1\beta_0^2}{k_2\gamma_0 Q} \ \mathrm{Im} \frac{1}{\Omega_\pm + \frac{1}{2}i\Gamma_\pm} , \tag{50c}$$

where

$$n_{ij}(\Delta_1/k_1) = N_i G_i(\Delta_1/k_1) - N_j G_j(\Delta_1/k_1) , \tag{51a}$$

$$W_{ij}(\Delta_1/k_1) = \frac{n_{ij}(\Delta_1/k_1)}{n_{ij}(0)} , \tag{51b}$$

$$R_j = \frac{2\pi}{k_1} \mid \alpha \mid^2 n_{0j}(0) , \tag{51c}$$

$$Q = (1 + 4\beta_0^2/\gamma_0\gamma_2)^{1/2} , \tag{51d}$$

$$\Omega_\pm = \Delta_1 \mp (k_1/k_2)\Delta_2 , \tag{51e}$$

$$\Gamma_\pm = \gamma_1 + \gamma_\pm Q , \tag{51f}$$

and

$$\gamma_\pm = \frac{k_1}{k_2}\gamma_2 + \frac{|k_2 \mp k_1|}{k_2}\gamma_0 . \tag{51g}$$

Equations (50), valid for large values of E_2, were first given in Paper I. Curves of $\langle R_{01} \rangle$ and $\langle R_{02} \rangle$ for the detuned case with $k_1 \geq k_2$ are plotted from Eqs. (43b) and (43c) in Figs. 6(a), 6(b), 6(e), 6(f), 7(c), and 7(d). It is found that the results agree with the analytical expressions, Eqs. (50). The $\langle R_{02} \rangle$ curves exhibit a pair of Lorentzian resonances of equal area at $\Omega_\pm = 0$, of widths $\Gamma_\pm$, as in Eq. (50c). Note that $\Gamma_\pm$ are significantly power broadened for intense laser fields ($Q \gg 1$), as in Eq. (51f). The + and − resonances correspond to the interaction of E_1 with the parallel (E_2^+) and antiparallel (E_2^-) components of E_2, respectively. The $\langle R_{01} \rangle$ curve exhibits no structure, in accord with Eq. (50b), and is identical to the background that one would observe if E_2 were absent.

Case 2. $k_1 < k_2$. In this case we find that

$$\langle R_{01} \rangle = \langle R_{01}^0 + R_{01}(+) \rangle = -R_1 W_{01}(\Delta_1/k_1)\mathrm{Im}(T/Y) , \tag{52a}$$

$$\langle R_{01}(-) \rangle = 0 , \tag{52b}$$

$$\langle R_{02}(-) \rangle = \text{same as for } k_1 \geq k_2 \text{ [Eq. (50c)]}, \tag{52c}$$

$$\langle R_{02}(+) \rangle = -2R_2 W_{02}(\Delta_1/k_1) \frac{\beta_0^2}{Q}\left(\frac{k_1}{k_2}\right)^2 \times \mathrm{Im}\left\{ Y^{-1}\left[\frac{1}{B_+}\left(\frac{1+Q}{2} + i\frac{k_1-k_2}{\gamma_0 k_1}(A_+ + \delta)\right) + \frac{1}{B_-}\left(\frac{1-Q}{2} + i\frac{k_1-k_2}{\gamma_0 k_1}(A_- + \delta)\right)\right]\right\} , \tag{52d}$$

where

$$S^2 = 4\frac{k_1}{k_2}\frac{k_2-k_1}{k_2}\beta_0^2 , \tag{53a}$$

$$T = \Omega_+ + \tfrac{1}{2}i(\gamma_+ + \gamma_1) , \tag{53b}$$

$$Y = [S^2 - T^2]^{1/2} , \tag{53c}$$

where Y is always chosen to be on the left-hand side of the complex plane,

$$A_\pm = [-k_2/2(k_2-k_1)](T \pm iY) + (\Delta_1 + i\gamma_{01}) , \tag{53d}$$

$$B_\pm = \pm A_\pm + (k_1/k_2)(i\gamma_{20}Q \mp \Delta_2) , \tag{53e}$$

$$\delta = [-k_1/(k_2-k_1)](\Delta_{21} - i\gamma_{21}) . \tag{53f}$$

As an example, curves of $\langle R_{02} \rangle$ and $\langle R_{01} \rangle$ for the case $k_1 = \frac{1}{2}k_2$ are plotted from Eqs. (43b) and (43c) in Figs. 6(c) and 6(d) and 7(c) and 7(d). The results agree with curves plotted for the analytic expressions, Eq. (52), and differ significantly from those for the case $k_1 \geq k_2$: The $\langle R_{02} \rangle$ curves still exhibit a Lorentzian resonance at $\Omega_- = 0$ of width Γ_- corresponding to the interaction of E_1 with E_2^-, just as for the case $k_1 \geq k_2$. However, the resonance at $\Omega_+ = 0$, corresponding to the interaction of E_1 with E_2^+, exhibits a splitting which increases with increasing field strength E_2 and vanishes in the limit of weakly saturating fields, where the resonance reduces to a Lorentzian of width Γ_+ (see following paragraph). In addition to the features in $\langle R_{02} \rangle$, structure in $\langle R_{01} \rangle$ also manifests itself. We see that a distinctly non-Lorentzian resonance appears at $\Omega_+ = 0$. This resonance features a central dip and broad wings peaking off center, in such a manner as to leave the area of the $\langle R_{01} \rangle$ background curve unaltered by the presence of E_2.

The resonance is a result of the interaction of E_1 with E_2^+, and as such is a traveling-wave effect. This effect, which occurs even for weakly saturating values of E_2, has recently been observed in Ref. 9. The splitting of the $\langle R_{02}\rangle$ resonance, which appears only for a strongly saturating value of E_2, is a new effect and has not yet been observed.

C. Intense Standing-Wave Field: Near Resonance $[\Delta_2/\gamma_{20} \approx (1+\frac{1}{2}I)^{1/2}]$

In the near-resonance case interference effects produce additional line-shape alterations. Examples, plotted from Eqs. (43b) and (43c), are given in Figs. 8(a) and 8(b). Note that these curves combine features of the off-resonance and on-resonance cases, leading to complex asymmetric line shapes.

D. Limit of Weakly Saturating Laser Field ($Q \approx 1$)

The results for the case of weakly saturating laser are plotted in Fig. 7. The analytical expressions for the case $k_1 \gtrsim k_2$ are the same as in Eqs. (50) but with $Q = 1$, indicating that the Lorentzian resonances of different width but of equal area occur in $\langle R_{02}\rangle$ even in this limit. It follows from Eqs. (43b) and (43c) that in the weak saturation limit Eqs. (50) are valid even when the laser is tuned to the line center.

In this limit it follows from Eqs. (52) that the analytical results for the case $k_1 < k_2$ are identical to the results for $k_1 \gtrsim k_2$ with the exception of $\langle R_{01}(+)\rangle$, which is given by[23–25]

$$\langle R_{01}(+)\rangle = 2R_1 W_{01}(\Delta_1/k_1)\beta_0^2\left(\frac{k_1}{k_2}\right)\frac{k_2-k_1}{k_2} \times \mathrm{Re}\left[\frac{1}{\Omega_+ + i(\gamma_+ + \gamma_1)/2}\right]^2, \quad k_2 > k_1 . \quad (54)$$

Therefore, even for a weakly saturating laser field, structure appears on the background line shape when $k_2 > k_1$, although the area under $\langle R_{01}\rangle$ remains independent of E_2. No such structure appears when $k_1 > k_2$. Note also that the splitting of the narrow resonance of the $\langle R_{02}\rangle$ curves, which occurs at intense laser fields for $k_2 > k_1$, disappears in this limit. All these remarks are contingent upon the assumption that the Doppler widths are much greater than the natural widths.

Computer plots of Eq. (43) for $I = 0.1$ are given in Figs. 7(c) and 7(d) for the off-resonance case and Figs. 7(a) and 7(b) for the on-resonance case. Note that the latter curves are just the superposition at $\Delta_1 = 0$ of the detuned resonances, indicating that spatial interference effects between components of the induced polarization at Ω_1 are not significant here.

V. EQUAL AREA PROPERTY

Some interesting properties of the laser-induced change signals emerge from the results presented here. First, as stated above, the area under the $\langle R_{01}\rangle$ background is always independent of E_2. Secondly, the area under the $\langle R_{02}\rangle$ line shape is independent of the field interactions between E_1 and E_2. From this consideration it follows that when the laser is detuned the broad and narrow resonances are always equal in area, even when the narrow resonance splits in two. In fact, it may be shown that in each case the area under the exact line-shape curve [Eq. (43a)] is identically equal to that under the corresponding IFA curve [Eq. (45)]. This property is a manifestation of the fact, first pointed out by Javan,[31] that the area under the response of each *individual atomic velocity ensemble* is equal to that obtained from the corresponding IFA, even though the actual frequency behavior differs significantly. These results can be shown to follow from an elementary quantum-mechanical analysis of the transition rates of three-level systems coupled to applied fields. A detailed discussion will be deferred to a later paper.

ACKNOWLEDGMENTS

This work has benefitted from discussions with Professor Ali Javan and his support of the research. We are grateful to Irving P. Herman for a careful reading of the manuscript.

APPENDIX A: SOLUTION TO EQS. (33)

Consider the coupled nonhomogeneous linear difference equations, Eqs. (33) of the text, which may be written in the form

$$x_\pm(n+1) - x_\pm(n-1) + A_\pm(n)\,x_\pm(n) = \phi_\pm(n), \quad n \geq 1 \quad \text{(A1a)}$$

$$x_+(1) - x_-(1) + A(0)x(0) = \phi(0) , \quad \text{(A1b)}$$

$$x_+(0) = x_-(0) \equiv x(0) , \quad \text{(A1c)}$$

where

$$A_\pm(n) = \pm\,(1/i\beta_0)L(\pm n) , \quad \text{(A2a)}$$

$$\phi_\pm(n) = (\pm n_{02}/i\beta_0)\,t_\pm(n) , \quad \text{(A2b)}$$

$$A(0) = (1/i\beta_0)L(0) , \quad \text{(A2c)}$$

$$\phi(0) = (1/i\beta_0)t(0) . \quad \text{(A2d)}$$

Note that adjacent $x_\pm(n)$'s are coupled together in three's. The $\phi_\pm(n)$'s are prescribed driving terms. Equations (A1b) and (A1c) serve to join the $x_+(n)$ with the $x_-(n)$. Henceforth, the $\pm$ subscripts will be deleted when convenient.

The solution to Eqs. (A1) may be formed from the solutions to the associated homogeneous equations, $x^H(n)$. The homogeneous equations are obtained by setting the $\phi(n) = 0$:

$$x^H(n+1) - x^H(n-1) + A(n)x^H(n) = 0, \quad n \geq 1 . \quad \text{(A3)}$$

Solutions to equations of the type (A3) are discussed in detail in Sec. 5 of Ref. 21. A brief account is given here in Appendix B, where it is shown that the most general solution for $x^H(n)$ may be written in the form

$$x^H(n) = Cu(n) + Dv(n) , \quad \text{(A4)}$$

where $u(n)$ and $v(n)$ separately satisfy Eq. (A3), and C and D are arbitrary constants independent of n. The $u(n)$'s and $v(n)$'s are distinct classes of solutions characterized by their behavior at large n. The $u(n)$'s, which we call B-type solutions, have the limiting behavior

$$u(n) \sim \frac{1}{n!}\left(\frac{\beta_0}{ik_2 v}\right)^n , \quad n \text{ large.} \quad \text{(A5a)}$$

The $v(n)$'s, called N-type solutions, have the limiting behavior

$$v(n) \sim (n-1)!\ (k_2 v/i\beta_0)^n , \quad n \text{ large.} \quad \text{(A5b)}$$

Accordingly, in the limit $n \to \infty$, $u(n)$ vanishes whereas $v(n)$ diverges. In subsequent discussions it will be convenient to normalize $u(n)$ and $v(n)$ such that

$$u(0) = v(0) = 1 . \quad \text{(A6)}$$

Solutions to the nonhomogeneous equations (A1a) may be constructed using the method of variation of parameters.[32] Let us assume $x(n)$ to be of the form

$$x(n) = C(n)u(n) + D(n)v(n), \quad n \geq 0 . \quad \text{(A7)}$$

Inserting Eq. (A7) into Eq. (A1), and eliminating terms containing $A(n)$ by means of Eq. (A3), one obtains, for $n \geq 1$,

$$\delta C(n)u(n+1) + \delta D(n)v(n+1) + \delta C(n-1)u(n-1) + \delta D(n-1)v(n-1) = \phi(n) , \quad \text{(A8)}$$

with

$$\delta C(n) = C(n+1) - C(n) , \quad \text{(A9a)}$$

$$\delta D(n) = D(n+1) - D(n) . \quad \text{(A9b)}$$

Trial solution (A7) does not uniquely specify the $C(n)$'s and $D(n)$'s, and in Eq. (A8) we are free to choose

$$\delta C(n)u(n) + \delta D(n)v(n) = 0, \quad n \geq 0 \quad \text{(A10)}$$

whereupon for $n \geq 1$,

$$\delta C(n)u(n+1) + \delta D(n)v(n+1) = \phi(n) . \quad \text{(A11)}$$

Combining Eqs. (A10) and (A11), we find

$$\left.\begin{aligned} \delta C(n) &= \frac{\phi(n)v(n)}{u(n+1)v(n) - u(n)v(n+1)} \quad \text{(A12a)} \\ \delta D(n) &= \frac{-\phi(n)u(n)}{u(n+1)v(n) - u(n)v(n+1)} \quad \text{(A12b)} \end{aligned}\right\} n \geq 1 .$$

These expressions may be simplified by means of the following identity, obtained from Eq. (A3):

$$\begin{aligned} u(n+1)v(n) - v(n+1)u(n) &= -[u(n)v(n-1) - v(n)u(n-1)] \\ &= (-1)^n[u(1) - v(1)] . \end{aligned} \quad \text{(A13)}$$

(The last step follows by induction.) Thus,

$$\left.\begin{aligned} \delta C(n) &= \frac{(-1)^n \phi(n)v(n)}{u(1) - v(1)} \quad \text{(A14a)} \\ \delta D(n) &= -\frac{(-1)^n \phi(n)u(n)}{u(1) - v(1)} \quad \text{(A14b)} \end{aligned}\right\} n \geq 1 .$$

Accordingly, for $n > 1$,

$$C(n) = C(1) + \frac{1}{u(1) - v(1)} \sum_{j=1}^{n-1} (-1)^j \phi(j)v(j) , \quad \text{(A15a)}$$

$$D(n) = D(1) - \frac{1}{u(1) - v(1)} \sum_{j=1}^{n-1} (-1)^j \phi(j)u(j) . \quad \text{(A15b)}$$

An additional equation, obtainable from Eq. (A10) for $n = 0$, is

$$C(0) + D(0) = C(1) + D(1) \quad \text{(A16)}$$

since, by Eq. (A6),

$$u(0) = v(0) = 1 . \quad \text{(A17)}$$

Therefore, using Eq. (A6), we can write down the sequence

$$x(0) = C(1) + D(1) , \quad \text{(A18a)}$$

$$x(1) = C(1)u(1) + D(1)v(1) , \quad \text{(A18b)}$$

$$x(n) = \left(C(1) + \frac{1}{u(1) - v(1)} \sum_{j=1}^{n-1} (-1)^j \phi(j)v(j)\right) u(n) + \left(D(1) - \frac{1}{u(1) - v(1)} \sum_{j=1}^{n-1} (-1)^j \phi(j)u(j)\right) v(n), \quad n \geq 1. \quad \text{(A18c)}$$

Thus the $x(n)$'s may be expressed in terms of two quantities independent of n, $C(1)$ and $D(1)$, as yet undetermined.

The value of $D(1)$ may be established by considering the behavior of $x(n)$ as $n \to \infty$. Recall from Sec. II that the $x(n)$'s are the coefficients of Fourier expansions in $k_2 z$ for ρ'_{21} and ρ'_{01}. The latter quantity is essentially the induced polarization at Ω_1; consequently the emitted power ΔI may be expressed as a sum of $x(n)$'s (n even) [Eq. (31)]. For all physically possible (i.e., finite) values of $\phi(n)$, ΔI must remain finite; hence the $x(n)$'s may not diverge. [It was shown in Ref. 21 that the $\phi(n)$'s themselves strongly converge to 0 as $n \to \infty$; see also Table I.]

This requirement on $x(n)$ places a restriction on

the coefficient of $v(n)$ in Eq. (A18c). Note first that in Eq. (A18c) both summation terms [including multiplication by $u(n)$ or $v(n)$, respectively] converge rapidly to zero for n large. Thus, since $u(n)$ itself converges $\sim 1/n!$ [Eq. (A5a)], the entire first bracketed term of Eq. (A18c) converges. But, as can be seen in Eq. (A5b), $v(n)$ diverges $\sim (n-1)!$, placing a restriction on its coefficient. In fact, the required boundary condition can only be guaranteed by setting

$$D(1)=\frac{1}{u(1)-v(1)}\sum_{j=1}^{\infty}(-1)^j\phi(j)u(j)\,. \tag{A19}$$

The remaining constant, $C(1)$, may now be determined. Displaying the subscripts as in Eq. (A1), we have from Eq. (A1b)

$$x_+(1)-x_-(1)+A(0)x(0)=\phi(0)\,, \tag{A20a}$$

from Eq. (A18b)

$$x_+(1)=C_+(1)u_+(1)+D_+(1)v_+(1)\,, \tag{A20b}$$

$$x_-(1)=C_-(1)u_-(1)+D_-(1)v_-(1)\,, \tag{A20c}$$

and from Eqs. (A18a) and (A1c)

$$x(0)=C_+(1)+D_+(1)\,, \tag{A20d}$$

$$x(0)=C_-(1)+D_-(1)\,. \tag{A20e}$$

These equations may be routinely combined to obtain

$$x(0)=\frac{\phi(0)+\sum_{j=1}^{\infty}(-1)^j\{\phi_+(j)u_+(j)-\phi_-(j)u_-(j)\}}{u_+(1)-u_-(1)+A(0)}\,. \tag{A21}$$

Substitution of definitions (A2) gives the result of Eq. (37) of the text.

Rate-Equation Approximation

The rate equation approximation (REA) for a two-level system interacting with a standing-wave field is that approximation in which spatial population variations arising from the interaction are neglected. In extending this approximation to a three-level system we ignore contributions of the polarization arising from these terms (i.e., $x_n=0, n>1$). The difference equations [Eq. (A1a)–(A1c)] considerably simplify and we have

$$-x(0)+A_\pm(1)x_\pm(1)=\phi_\pm^{\mathrm{REA}}(1)\,, \tag{A22a}$$

$$x_+(1)-x_-(1)+A(0)x(0)=\phi^{\mathrm{REA}}(0)\,. \tag{A22b}$$

Solving these equations directly, we find

$$x^{\mathrm{REA}}(0)=\frac{\phi^{\mathrm{REA}}(0)+\phi_-^{\mathrm{REA}}(1)/A_-(1)-\phi_+^{\mathrm{REA}}(1)/A_+(1)}{A(0)+1/A_+(1)-1/A_-(1)}\,, \tag{A23}$$

where the $\phi^{\mathrm{REA}}(n)$ are obtained from Eq. (A2) and Eq. (35), using the REA values from Table I, Eqs. (T20)–(T22).

APPENDIX B: SOLUTION OF EQ. (A3)

Consider Eq. (A3):

$$x_\pm^H(n+1)-x_\pm^H(n-1)+A_\pm(n)x_\pm^H(n)=0,\quad n\geq 1 \tag{B1}$$

where

$$A_\pm(n)=\pm(1/i\beta_0)L(\pm n)\,, \tag{B2}$$

$$L(\pm n)=\begin{cases}\Delta_{12}-(k_1\pm nk_2)v+i\gamma_{21}, & n \text{ odd}\\ \Delta_1-(k_1\pm nk_2)v+i\gamma_{10}, & n \text{ even}\end{cases}\,. \tag{B3}$$

In second-order homogeneous difference equations, such as Eq. (B1), one may distinguish two classes of solutions, characterized by the behavior of $x^H(n)$ for large values of n.[21] In the present case the nature of these types of solutions is readily ascertained, noting that for large enough n (for $v\neq 0$),

$$L(\pm n)\to\mp nk_2v\,, \tag{B4}$$

so that

$$A_\pm(n)\to(ik_2v/\beta_0)n\,. \tag{B5}$$

To obtain the first class of solutions, assume that for large n

$$x_\pm^H(n+1)\gg x_\pm^H(n-1)\,. \tag{B6}$$

Then

$$\frac{x_\pm^H(n+1)}{x_\pm^H(n)}\sim\frac{k_2v}{i\beta_0}\,n\,, \tag{B7}$$

so that

$$x_\pm(n)\propto(n-1)!\,(k_2v/i\beta_0)^n\,. \tag{B8}$$

Note that $x_\pm(n)\to\infty$ for large n, in accord with initial assumption (B6). We denote solutions of this type by $v_\pm(n)$. Because of their close connection with Neumann functions we refer to solutions of the latter type as N-type solutions.[21]

The second class of solutions is obtained by assuming

$$x_\pm^H(n-1)\gg x_\pm^H(n+1)\,. \tag{B9}$$

Then

$$\frac{x_\pm^H(n)}{x_\pm^H(n-1)}\sim\frac{\beta_0}{ik_2v}\,\frac{1}{n}\,, \tag{B10}$$

so that

$$x_\pm(n)\propto\frac{1}{n!}\left(\frac{\beta_0}{ik_2v}\right)^n\,. \tag{B11}$$

Note that $x_\pm(n)\to 0$ for large n, in accord with initial assumption (B9). These convergent solutions are denoted by $u_\pm(n)$. Because of their close connection with Bessel functions we refer to solutions of this type as B-type solutions.[21]

To express $u_\pm(n)$ in a form convenient for computation we define the quantity

$$W_{\pm}(n) = u_{\pm}(n)/u_{\pm}(n-1) \ . \tag{B12}$$

Then from Eq. (B1) we obtain an expression for $W_{\pm}(n)$ in continued-fraction form:

$$W_{\pm}(n) = \cfrac{\pm i\beta_0/L[\pm n]}{1 - \cfrac{\beta_0^2/L[\pm n]\,L[\pm(n+1)]}{1 - \cfrac{\beta_0^2/L[\pm(n+1)]L[\pm(n+2)]}{1 \pm i\beta_0 W_{\pm}(n+3)/L[\pm(n+2)]}}} \ . \tag{B13}$$

Then

$$u_{\pm}(n) = \prod_{k=1}^{n} W_{\pm}(k) \ , \tag{B14}$$

where we have set $u_{\pm}(0) = 1$ without loss of generality.

Special Case: $\gamma_2 = \gamma_0$ *and* $\Delta_2 = 0$. For the case $\gamma_2 = \gamma_0$ and $\Delta_2 = 0$, $u_{\pm}(n)$ may be written analytically in terms of $J_{\tau}(z)$, the Bessel function of real argument z and complex order τ:

$$u_{\pm}(n) = \frac{i^n J_{\tau(n)}(-2\beta_0/k_2 v)}{J_{\tau(0)}(-2\beta_0/k_2 v)} \ , \tag{B15}$$

where

$$\tau(n) = \mp L(\pm n)/k_2 v \ . \tag{B16}$$

As before, Eq. (B15) is normalized such that $u_{\pm}(0) = 1$. Equation (B15) follows from Eq. (B1) which, in this special case, reduces to the well-known recurrence relation for cylindrical functions.[21]

APPENDIX C: ALGORITHM FOR COMPUTING CONTINUED FRACTIONS

Let

$$C = \cfrac{a_1}{1 + \cfrac{a_2}{1 + \cfrac{a_3}{1 + \ddots}}} \tag{C1}$$

Define

$$\frac{P_n}{Q_n} = \cfrac{a_1}{1 + \cfrac{a_2}{1 + \cfrac{a_3}{1 + \ddots \cfrac{}{1 + a_n}}}} \ . \tag{C2}$$

One can then show that P_n and Q_n obey the following difference equations:

$$P_n = P_{n-1} + a_n P_{n-2} \ , \tag{C3a}$$

$$Q_n = Q_{n-1} + a_n Q_{n-2} \ , \tag{C3b}$$

with

$$P_{-1} = 1, \quad P_0 = 0 \ , \tag{C3c}$$

$$Q_{-1} = 0, \quad Q_0 = 1 \ . \tag{C3d}$$

From the recurrence relations for P_n and Q_n one can readily compute P_n and Q_n for any value of n. The computation is halted when

$$\left| \frac{P_{n+1}/Q_{n+1} - P_n/Q_n}{P_n/Q_n} \right| < 10^{-6} \ . \tag{C4}$$

We then set

$$C = P_{n+1}/Q_{n+1} \ . \tag{C5}$$

---

*Work supported by Air Force Cambridge Research Laboratories, National Aeronautics and Space Administration, and Office of Naval Research.

[1]H. R. Schlossberg and A. Javan, Phys. Rev. 150, 267 (1966).

[2]H. K. Holt, Phys. Rev. Letters 19, 1275 (1967).

[3]T. Ya Popova, A. K. Popov, S. G. Rautian, and R. I. Sokolovskii, Zh. Eksperim. i Teor. Fiz. 57, 850 (1969); 57, 2254(E) (1970) [Sov. Phys. JETP 30, 466 (1970); 30, 1208 (1970)].

[4]M. S. Feld and A. Javan, Phys. Rev. 177, 540 (1969). This paper shall be referred to subsequently as I. The notation of the present paper is consistent with that of Paper I.

[5]T. Hansch and P. Toschek, Z. Physik 236, 213 (1970).

[6]J. A. White and R. Bose, Bull. Am. Phys. Soc. 13, 172 (1968).

[7]H. K. Holt, Phys. Rev. Letters 20, 410 (1968).

[8]I. M. Beterov and V. P. Chebotaev, Zh. Eksperim. i Teor. Fiz. Pis'ma v Redaktsyu 9, 216 (1969) [Sov. Phys. JETP Letters 9, 127 (1969)].

[9]T. Hansch, R. Keil, A. Schabert, Ch. Schmelzer, and P. Toschek, Z. Physik 226, 293 (1969); T. Hansch, Ph. D. thesis (University of Heidelberg, Germany, 1969) (unpublished).

[10]M. S. Feld, B. J. Feldman, and A. Javan, Bull. Am. Phys. Soc. 12, 669 (1967); L. H. Domash, M. S. Feld, B. J. Feldman, and A. Javan (unpublished).

[11]T. Ducas, M. S. Feld, L. W. Ryan, Jr., N. Skribanowitz, and A. Javan, Phys. Rev. A (to be published).

[12]R. H. Cordover, P. A. Bonczyk, and A. Javan, Phys. Rev. Letters 18, 730 (1967).

[13]M. S. Feld, Ph. D. thesis (MIT, 1967) (unpublished). See also Ref. 10.

[14]H. R. Schlossberg and A. Javan, Phys. Rev. Letters 17, 1242 (1966).

[15]J. S. Levine, P. A. Bonczyk, and A. Javan, Phys. Rev. Letters 22, 267 (1969).

[16]G. W. Flynn, M. S. Feld, and B. J. Feldman, Bull. Am. Phys. Soc. 12, 669 (1967).

[17]I. M. Beterov, Yu. A. Matyugin, and V. P. Chebotaev, Zh. Eksperim. i Teor. Fiz. Pis'ma v Redaktsyu 10, 296 (1969) [Sov. Phys. JETP Letters 10, 187 (1969)].

[18]T. Hansch and P. Toschek, IEEE J. Quantum Electron. 4, 467 (1968).

[19]W. G. Schweitzer, Jr., M. M. Birky, and J. A. White, J. Opt. Soc. Am. 57, 1226 (1967).
[20]S. Stenholm and W. E. Lamb, Jr., Phys. Rev. 181, 618 (1969).
[21]B. J. Feldman and M. S. Feld, Phys. Rev. A 1, 1375 (1970).
[22]The explanation of the velocity fine structure is discussed in detail in Ref. 21.
[23](a) T. Ya. Popova, A. K. Popov, S. G. Rautian, and R. I. Sokolovskii, in Proceedings of the National Symposium on the Physics of Gas Lasers, Novosibirsk, U.S.S.R., 1969 (unpublished); (b) A. K. Popov, Zh. Eksperim. i Teor. Fiz. 58, 1623 (1970) [Sov. Phys. JETP 31, 870 (1970)].
[24]T. Hansch and P. Toschek, in Ref. 23(a); see also Ref. 5.
[25]M. S. Feld, in Ref. 23(a).
[26]See Appendix C 3 of Paper I.
[27]See Paper I, Sec. III B for further discussion.
[28]The notation used in this paper is the same as that of Paper I. Note in Eq. (1b) that the magnitude of each traveling-wave components of $E_2(z,t)$ is E_2^0.
[29]Narrower velocity distributions, both rectangular and Gaussian, were found to produce small variations in the line shapes. See also G. E. Notkin, S. G. Rautian, and A. A. Feoktistov, Zh. Eksperim. i Teor. Fiz. 52, 1673 (1967) [Sov. Phys. JETP 25, 1112 (1967)].
[30]The integrations can be done by contour integration or by the method of partial fractions. See, for example, Appendix D of Paper I.
[31]A. Javan, Phys. Rev. 107, 1579 (1957).
[32]F. B. Hildebrand, *Finite Difference Equations and Simulations* (Prentice Hall, Englewood Cliffs, New Jersey, 1968).

PHYSICAL REVIEW A VOLUME 5, NUMBER 2 FEBRUARY 1972

Structural Absorption of Ultrasonic Waves in Associated Liquids

Gulshan Rai, B. K. Singh, and O. N. Awasthi
Department of Physics, University of Allahabad, Allahabad, India
(Received 9 July 1971)

Hall's modified theory of structural relaxation is applied to explain the pressure dependence of excess absorption in water, methanol, and ethanol in the pressure range 1–5000 kg/cm^2. An excellent agreement has been found between the theoretically calculated structural absorption and experimentally observed excess absorption for these three associated liquids. The values of structural compressibility β_r, structural relaxation time τ, and the free-energy difference ΔF between the two states assumed nearly coincide with their corresponding values in the range 1–2000 kg/cm^2 predicted in previous papers, and beyond this ($p > 2000$ kg/cm^2) the values are the same as would be expected by extrapolation of earlier curves up to 5000 kg/cm^2. This gives strong support to the two-state model and the assumptions made therein to explain absorption results in water, methanol, and ethanol.

I. INTRODUCTION

The occurrence of excess ultrasonic absorption in associated liquids has been successfully explained by attributing it to a structural relaxation mechanism, first proposed by Hall.[1] By assuming two types of structures which differ in molal volumes by an amount ΔV cm^3/mole and in molal free energy by an amount ΔF cal/mole, Hall explained the excess absorption in water in terms of transition of molecules from one type of structure to another under the influence of periodic variations of pressure and temperature associated with the ultrasonic waves propagating through the bulk of the liquid. A finite time is involved in the transitional jumps and hence the process is a relaxational one. For water, the two types of structures assumed are (i) icelike or open-packed structure, and (ii) close-packed structure. The former is supposed to be endowed with relatively higher molal volume and lower molal free energy than the latter. This assumption gave excellent agreement between theory and experiment for the temperature dependence of absorption in water,[1] heavy water,[2] and alcohols.[3,4] Litovitz and Carnevale[5] measured ultrasonic absorption in water as a function of pressure. Their results showed a decrease in excess absorption with increasing pressure while Hall's theory in its original form predicts an increase in excess absorption with pressure. The observed pressure dependence could, however, be explained if the open-packing state is tacitly assumed to be the higher energy state (which was provisionally assumed by Hall to be the lower energy state). With this modification and assumed linear variation of ΔV and ΔF with pressure, Litovitz and Carnevale successfully explained absorption results in water at 0 and 30 °C for the pressure range 1–2000 kg/cm^2.

Later, Carnevale and Litovitz[6] tried to explain their experimental results in methanol on similar grounds, but their calculated values were nearly 40% higher than the experimental values at intermediate pressures. This anomaly was removed by Kor *et al.*[7] by considering a nonlinear variation of